Journal of Hydrology: Regional Studies 41 (2022) 101076

Contents lists available at ScienceDirect

Journal of Hydrology: Regional Studies

journal homepage: www.elsevier.com/locate/ejrh

Projected increases in potential groundwater recharge and reduced evapotranspiration under future climate conditions in West Africa

P.A. Cook [a,*], E.C.L. Black [a], A. Verhoef [b], D.M.J. Macdonald [c], J.P.R. Sorensen [c]

[a] NCAS-Climate, Department of Meteorology, University of Reading, UK
[b] Department of Geography and Environmental Science, University of Reading, UK
[c] British Geological Survey, UK

ARTICLE INFO

Keywords:
West African monsoon
Soil water balance
CO_2 fertilisation
Land use change
Water resources

ABSTRACT

Study region: West Africa, with a focus between 5°W and 5°E.
Study focus: The effects of changing climate and CO_2 concentration (RCP8.5 between 2000 and 2100) on the West African monsoon are examined using the UPSCALE high-resolution (25 km) global climate model ensembles for present and future climate, combined with the JULES land-surface model.
New hydrological insights: Future climate is predicted to have an enhanced summertime Saharan heat low, changing large-scale circulation, causing monsoon rainfall generally to increase. The monsoon progresses further inland and occurs later in the year. UPSCALE rainfall projections indicate that the eastern Sahel becomes wetter (+ 12.2%) but the western Sahel drier (− 13.5%). Future evapotranspiration is reduced across most of West Africa due to the CO_2 fertilisation effect causing lower transpiration. Potential groundwater recharge (soil drainage at the bottom of a 3 m deep soil column), is predicted to increase from 0% to 16% of rainfall under present climate, to 1–20% in the future, doubling from ~ 5% to ~ 10% in northern Ghana and the eastern Sahel. Potential recharge increases largely due to increased soil hydraulic conductivity, caused by higher soil moisture resulting from increased rainfall and reduced transpiration. Other factors have only a minor influence on the water balance and potential recharge, including rainfall intensity and land use type. A predicted increase in future potential groundwater recharge is significant as development of groundwater resources is seen as a key means to meet growing water demand in West Africa.

1. Introduction

The West African summer monsoon is caused by the Saharan heat low setting up a southwest to northeast air flow from the coast to the Sahel which brings moist air from the Atlantic to provide rainfall from June to September each year (Meynadier et al., 2010a, 2010b; Marsham et al., 2013); the coastal region sees a bimodal monsoon. The monsoon is vital for the population of the region, with the rainfall providing the seasonal influx to terrestrial water resources to support drinking water sources, agricultural production, and economic development (Coulibaly et al., 2018; Naabil et al., 2017; Ascott et al., 2020).

* Correspondence to: NCAS-Climate, Department of Meteorology, University of Reading, Earley Gate, PO Box 243, Reading RG6 6BB, UK.
E-mail address: peter.raphalge@gmail.com (P.A. Cook).

https://doi.org/10.1016/j.ejrh.2022.101076
Received 24 February 2021; Received in revised form 30 March 2022; Accepted 4 April 2022
Available online 22 April 2022

There is a substantial body of research demonstrating that characteristics of the monsoon have already changed over recent decades. Most of the West African rain is from mesoscale convective systems, and Taylor et al. (2017) used satellite observations to show an increased frequency of extreme storms in the Sahel between 1982 and 2016 due to an increased south-north temperature gradient. Previously, Panthou et al. (2014) used rain gauge data from a network of 43 stations to show Sahelian rainfall has an increasing fraction of extreme rainfall (defined as occurring < 2.5 times per year on average at any station). More recently, Panthou et al. (2018) used a large set of daily rain gauge data (1950 onwards), with 5-min rain observations from the AMMA-CATCH Niger observatory since 1990, to find increased mean intensity of rainy days and higher frequency of heavy rainfall in the Sahel; a new era of extremes since 2000, and a stronger increase in extreme rain in east Sahel than in the west. Moreover, Dardel et al. (2014) used the GIMMS-3g NDVI dataset between 1981 and 2011 and found statistically significant increases in rainfall over almost all the Sahel, with long-term field observations showing re-greening in places. Odoulami and Akinsanola (2018) examined West African monsoon daily rainfall trends measured by GPCP and TRMM during 1998–2013, finding reduced rainfall in the region of Guinea and increased rainfall in the Sahel. Bichet and Diedhiou (2018), using the CHIRPS dataset at 0.05° resolution over 1981–2014, found that the West African Sahel has become wetter, principally from the number of wet days (+ 10 days compared to the normal) over the entire Sahel band, along with an increase in intensity over the central part (+ 3 mm/day). They also found that although dry spells are also becoming more frequent these are on average shorter (by 30%) over the entire Sahel band so do not represent a reduction in rainfall, and that precipitation intensity in the west (Senegal) has decreased (by around 3 mm/day). Sacre Regis et al. (2020) used CHIRPS data over 1986–2015 finding increased precipitation and more wet days in the west and central Sahel.

Various researchers have also explored how the West African monsoon is likely to change under future climate projections, using both regional and global climate models. Global modelling studies have generally found that rainfall over West Africa increases in the east, with some models projecting decreases over the west. Maynard et al. (2002), for example, used the Meteo-France climate model (ARPEGE-Climate), at a resolution of 312 km, to predict the impact of increasing greenhouse gases and aerosols on precipitable water, water vapour recycling, moisture convergence and precipitation efficiency. They reported an enhanced monsoon precipitation at the end of the twenty-first century, and changes in the position and strength of the African Easterly Jet, and the Hadley and Walker circulations. Kamga et al. (2005) compared the National Center for Atmospheric Research (NCAR) coupled atmosphere-ocean climate system model (CSM) simulation, at 312 km resolution, to long-term observations and to the National Centers for Environmental Prediction (NCEP) reanalysis, finding increases in West Africa summer (JJA) temperatures of 1.5–2.5 C between 1951 and 1980 and the late 21st century. Also, they predicted that the Sahel would likely be wetter in the late 21st century with increased atmospheric moisture, stronger meridional winds from the Gulf of Guinea, and a slightly stronger AEJ. Roehrig et al. (2013) used results from the 5th Climate Model Intercomparison Project (CMIP5; resolutions between 0.25° and 2.8°) to examine future rainfall in the Sahel. They found that the Sahara has greater warming than land to the south, and a good model consensus on reduced future precipitation in the western Sahel (15–5W) and increased precipitation in the east (0–30 E).

The gross projected patterns in West African precipitation change are similar for regional climate models (RCMs) as for global climate models. Sylla et al. (2015) used results from ensembles of Earth System Models (ESMs) and Regional Climate Models (RCMs) at 25 km resolution, run for historical and future periods (RCP4.5 and RCP8.5), to study high-intensity daily precipitation events for West Africa. Their findings showed a good match between model rainfall estimates and rainfall statistics derived from TRMM and GPCP for present conditions and predicted a delay in monsoon onset in the future, combined with more intense rainfall events due to stronger moisture convergence, particularly in RCP8.5 and more so over the Sahel than further south. Diallo et al. (2016) modelled the future monsoon with the regional climate model RegCM4 at 50 km resolution for 1970–2100 with driving data generated by HadGEM2-ES and MPI-ESM GCM (Global Climate Models) under the RCP8.5 greenhouse gas concentration pathway. They found changes to the African and Tropical Easterly Jets, a changing water budget with more extreme rainfall, and again a drier west but a wetter east Sahel. Todzo et al. (2019) used outputs from CORDEX-AFRICA, an ensemble of 18 high resolution (50 km) regional climate projections (RCP8.5 over 2006–2099), to find an intensification of the hydrological cycle in West Africa. They found that temperatures are expected to rise faster here than the global average rate leading to more intense but less frequent rainfall with longer dry spells.

At the finest spatial resolution, Kendon et al. (2019) carried out climate change experiments with the CP4-A convection-permitting high-resolution (4.5 km) model for the first time over the Africa-wide domain, and projected greater future increases in extreme 3-hourly precipitation compared to a convection-parameterised 25 km model, but also future increases in dry spell length during the wet season over western and central Africa. Berthou et al. (2019) used results from CP4-A for the period 1997–2006 to improve simulations of the monsoon, resulting in increased moisture convergence in the Sahel, more short-lasting intense rainfall events (Mesoscale Convective Systems, MCSs), better representation of wet and dry spells (daily and sub-daily), and an improved diurnal cycle of rainfall which impacts the diurnal monsoon winds. Fitzpatrick et al. (2020) used results from CP4-A (RCP8.5 until 2100) and predicted a 28% increase of extreme rain rate MCSs in the Sahel, mostly due to greater total water columns (using Clausius-Clapeyron scaling but with regional heterogeneity), modulated by increased vertical wind shear.

When planning adaptation measures, it is crucial to assess precipitation change in the context of present day variability. A methodology for this is presented in Gaetani et al. (2020), which used 29 state-of-the-art climate models (0.5° resolution, ~ 50 km) to estimate the Time of Emergence (TOE) of precipitation changes in West Africa. They found a clear difference between west and east Sahel, and a reduced occurrence of wet days likely to emerge before 2036, and a possible drier climate during 2028–2052 in the west, but a wetter climate in the east with an increased occurrence of very wet days likely to emerge before 2054.

Increased rainfall does not necessarily lead to reduced irrigation demand. Sylla et al. (2018) applied a 23-member ensemble of RCPs (50 km resolution) to assess hydrological changes for West Africa under 2 °C and 1.5 °C global warming. They found increased irrigation demand but reduced water availability in 10 major river basins in the area, limiting sustainable agriculture in the 2 °C scenario, however impacts reduced by up to 50% in the 1.5 °C scenario.

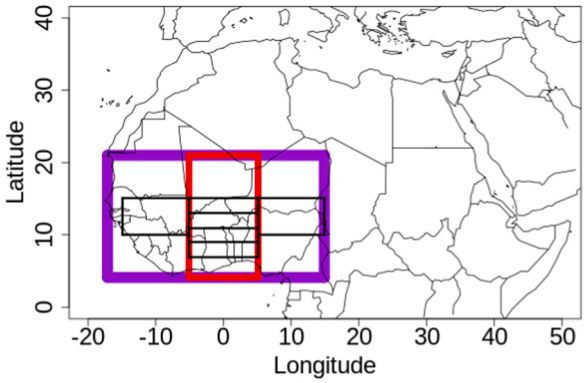

Fig. 1. Regions used in the analyses for this study. The entire domain modelled in this study (17 W to 15 E, 4–21 N) is indicated by the purple rectangle, and the central region (5 W to 5 E, 4–21 N) used for zonal means is delineated by the red rectangle. Also, the six sub-regions: four in the central region, referred to as southern Ghana (7–9 N), northern Ghana (9–11 N), southern Burkina Faso (11–13 N) and northern Burkina Faso (13–15 N); as well as one in the west Sahel (15–5 W, 10–15 N) and one in the east Sahel (5–15 E, 10–15 N), are indicated by black rectangles.

Any changes in future climate, encompassing variables such rainfall, temperature and vapour pressure deficit, will impact vegetation functioning. Moreover, the concurrent changes in atmospheric CO_2 concentration will also play an important role in plant physiological behaviour. The effects of elevated CO_2 concentrations on plant transpiration and water use efficiency have been known for many decades, and have mainly been studied empirically using a number of laboratory, in-situ and remote sensing techniques, as summarised in Kirschbaum and McMillan (2018). The general consensus is that photosynthesis will increase under elevated CO_2 concentrations, while the concurrent reduction in stomatal opening in most plants will cause a reduction in transpiration (Xu et al., 2016). The strength of this reduction will depend on climatic factors and soil water availability. The projected changes in transpiration will affect rain-forming processes. For example, Mengis et al. (2015) performed experiments with an intermediate complexity Earth System Climate Model (UVic ESCM; 3.6° resolution) for a range of model-imposed transpiration sensitivities to CO_2, and found that by 2100, under a high emission scenario, changing the sensitivity of transpiration to CO_2 caused a range of changes to the simulated terrestrial precipitation of − 10% to + 27%. Their study emphasises the importance of an improved assessment of the dynamics of environmental impact on vegetation to better predict future changes of the terrestrial hydrological and carbon cycles.

Any future changes in rainfall amount and timing during the monsoon have implications in terms of the West African terrestrial water balance and hence for water and food security. Much of the region is underlain by low storage and low productive aquifers, which are more susceptible to short term decreases in groundwater recharge resulting from lower rainfall than elsewhere in the continent (Adelana and MacDonald, 2008; Bianchi et al., 2020). Changes in rainfall intensity (Cuthbert et al., 2019) and land use change (Favreau et al., 2009) may also affect groundwater recharge.

The frequently dispersed communities also often rely on small reservoirs (UNECA, 2015), which have limited capacity and depend on more regular rainfall-driven inflows in semi-arid regions (Krol et al., 2011). In terms of food production, agriculture is predominantly rainfed (Sultan and Gaetani, 2016) and is highly dependent on seasonal rainfall (Cooper and Coe, 2011). This type of agriculture is the mainstay of rural livelihoods in this region and the primary source of food for the urban centres.

The study presented here represents a novel analysis of hydrological variability in West Africa (17 W to 15 E, 4–21 N) using an ensemble of high resolution (25 km) climate simulations (UPSCALE, see Section 2.1); this resolution is higher than that used in most other studies mentioned above, apart from that used in the convection-permitting studies. Previous work has shown that low resolution global coupled models represent the variability in precipitation poorly in this region because of biases in sea surface temperatures, SST (Dunning et al., 2017), and crude topography (Jung and Kunstmann, 2007). UPSCALE, in contrast, captures the variability well (Dunning et al., 2017; Black et al., 2021). This paper, furthermore, extends previous work on precipitation change (e.g., Roehrig et al., 2013) by considering the full water balance at the land surface, by using the UPSCALE near-surface atmospheric variables to drive the JULES land surface model. Also, the physiological impacts of climate change (via increases in CO_2 concentration) on vegetation functioning are explicitly considered, along with the implications for the terrestrial water balance; this effect has been little explored for West Africa.

Within the West African geographical domain, we focus on a central region which includes Burkina Faso and Ghana (5 W to 5 E), where rainfall patterns and vegetation and soil are fairly constant laterally across a series of zones; these zones provide a north-south transect through the Savanna and Sahel climate zones (Fig. 1). First, we discuss the key atmospheric variables relating to the large-scale circulation during the West African summer monsoon obtained from UPSCALE for current and future climates. Next, the resulting present and future rainfall, their daily intensity and the spatial and temporal patterns of the monsoon are presented and discussed, as well as the effects on the terrestrial water balance, with emphasis on the partitioning of precipitation water between evapotranspiration, surface runoff, potential recharge (soil drainage flux at the bottom of a 3 m deep soil column; we use 'potential' here because in reality some of this drainage flux may become interflow and hence will not recharge the aquifers) and soil moisture storage. Finally, the influence of vegetation cover on the present-to-future changes in the water balance, as well as the physiological response of the vegetation to increasing CO_2 concentrations, are analysed and discussed.

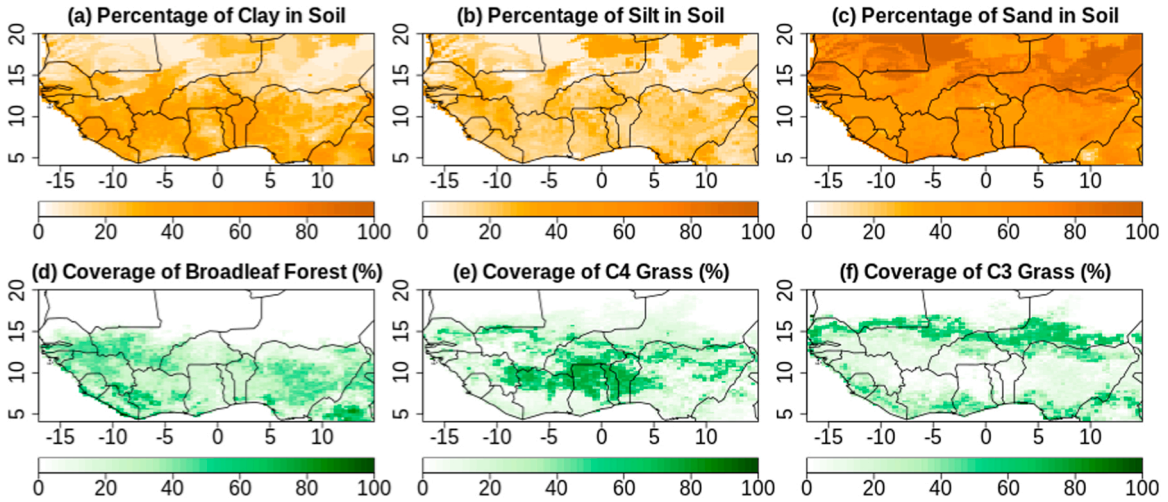

Fig. 2. Soil textural composition over West Africa expressed as percentages of clay, silt and sand; and vegetation coverage, as percentages of broadleaf trees, C4 grass and C3 grass.

2. Materials and methods

2.1. UPSCALE current and future climate data

In this study, data were taken from the UPSCALE (UK on PRACE: weather-resolving Simulations of Climate for globAL Environmental risk; Mizielinski et al., 2014) project high resolution (25 km) ensemble of climate simulations. These simulations are based upon the HadGEM3 Global Atmosphere 3 (GA3) and Global Land 3 (GL3) configurations of the UK Meteorological Office Unified Model (UM) and the Joint UK Land Environment Simulator (JULES) respectively, as documented in Walters et al. (2011). The UPSCALE simulations were forced with OSTIA SSTs and current atmospheric CO_2 concentration (5.241×10^{-4} kg/kg) for present climate (5 ensemble members covering 27 years between 1985 and 2011); and with OSTIA SSTs plus the anticipated SST change from 1990–2010 to 2090–2110 (in the HadGEM2 Earth System run under the IPCC Representative Concentration Pathway 8.5 climate change scenario) and increased CO_2 concentration (1.4217×10^{-3} kg/kg) for future climate (3 ensemble members, also for 27 years each). CO_2 concentration was kept constant during each 27-year run. The ensembles provide large datasets of simulated current and future climate for statistical studies. The land surface is prescribed a global emissivity of 0.97, while the albedo is set by the JULES land surface model. The global high resolution and large number of ensemble members of UPSCALE are expected to capture the details of the spatiotemporal distribution of atmospheric variables and large-scale circulation, in our case to allow for reliable simulation of the changes in the West African monsoon and terrestrial water balance under a changing climate. The UPSCALE outputs comprise a range of atmospheric outputs at different model levels; in our results section we present the near-surface data. Values for the potential evapotranspiration (*PET*) were not available from UPSCALE and were calculated using the Penman-Monteith equation (Allen et al., 1998) for our study.

2.2. Off-line distributed JULES runs driven with UPSCALE climate data

The daily atmospheric variables from UPSCALE were used to drive the JULES land-surface model (Best et al., 2011; Clark et al., 2011; Walters et al., 2011), version 4.1, that was provided with data on vegetation cover and soil texture (see Fig. 2) to produce model estimates of the terrestrial water balance and energy balance in West Africa. The driving variables are rainfall (*P*), mean air temperature, diurnal air temperature range, downwelling short- and longwave radiation, specific humidity, surface pressure and wind speed. JULES was run across West Africa in distributed fashion with (91×72) individual grid boxes, between 17°W and 15°E longitude (17 W to 15 E), and 4° and 21°N latitude (4–21 N). The land-surface model runs also allow us to study the response of plants to the changing climate and CO_2 concentration, which will affect the water balance, as well as model sensitivities with regards to vegetation type and coverage, as explained below.

For JULES, the UPSCALE daily data were disaggregated into hourly time steps. For each day the total rainfall is restricted to one event of duration τ (6 h for convective rain) which is placed at random in the day, provided there is a dry period of at least τ hrs before the end of the day; for especially extreme rainfall, greater than 350 mm/day, τ is increased. Air temperature is given a diurnal cycle, set by the daily mean and diurnal temperature range, with the maximum temperature occurring at 0.15 of a day (3 h and 36 min) after local noon. The downwelling radiation values are also given diurnal cycles, with longwave depending on the air temperature following Stefan Boltzmann's law (assuming black body radiation) while shortwave depends on the angle of the Sun above the horizon. Daily specific humidity is kept constant throughout the day except if the relative humidity reaches 100%, with saturated vapour pressure calculated from the hourly air temperature, in which case the humidity is limited to this value during these hours and hence is not

conserved. Both pressure and wind are kept constant throughout the day. In concordance with the UPSCALE runs, atmospheric CO_2 was also set to 5.241×10^{-4} kg/kg for present climate and 1.4217×10^{-3} kg/kg for future climate, although we also conducted JULES runs driven with future climate data, while atmospheric CO_2 was kept at present levels (see Section 2.3).

JULES has a prescribed vegetation seasonal cycle, based on a monthly climatology of leaf area index (see Clark et al., 2011). There are 4 soil layers (with thicknesses, starting at the surface, of 0.1, 0.25, 0.65, and 2.0 m, i.e., a soil profile of 3 m depth). Each gridbox is composed of nine 'tiles' with six of those vegetated (for each plant functional type a vegetation fractional coverage needs to be provided, as well as values for the plant parameters; see Clark et al., 2011). For each gridbox, the soil texture information provided by the soil map (Marthews et al., 2014 describes the soil data used in JULES; see also Fig. 2) has been used to calculate values for key soil parameters, such as those relating to soil water flow, the so-called soil hydraulic parameters; i.e., saturated hydraulic conductivity (K_{sat}), and the field capacity (referred to as 'critical' point as JULES uses a value of − 33 kPa to set this point) and wilting point, two key soil moisture values on the water retention curve. JULES was configured by selecting the Brooks and Corey (1964; from here on referred to as BC) soil hydraulic model, with any excess water being 'pushed up' if a soil layer becomes saturated.

As described in Section 2.1, the UPSCALE runs included JULES to simulate the interactions between the land surface and the atmosphere, however, the GL3 configuration used during the UPSCALE project invoked the Van Genuchten (VG) soil hydraulic scheme (Van Genuchten, 1980), which has been reported to cause JULES to produce very low values for infiltration and potential recharge for certain soil types and conditions. This is because there is a discrepancy in the shape of the water retention curves at the wet end, between the BC and VG equations. This discrepancy causes unsaturated soil hydraulic conductivity (at medium to high soil moisture contents) to be underestimated when the VG parameters are approximated from the BC-specific soil parameters, as is currently standard practice among JULES users (and was also the case for GL3). While this concerns standard conversions between the shape parameters of both hydraulic approaches, these are known to provide suboptimal parameter estimates near saturation. Hence, for our off-line study, JULES was run with the BC soil hydraulic scheme to obtain more realistic values for potential groundwater recharge. We conducted some preliminary tests with the JULES model where we compared hydrological flux outputs with either the VG or the BC hydraulic scheme invoked. We found that with the BC scheme less runoff and more potential recharge was produced (in fact with the VG scheme switched on hardly any drainage was produced). The amounts of potential recharge simulated based on the JULES-BC runs were comparable to those found in the literature for the geographical areas under consideration. This was the main reason for choosing BC over VG in our JULES model runs.

The JULES terrestrial water balance outputs comprised the sum of direct evaporation from the soil (E_s) and transpiration from the plants (T), evaporation from the canopy ('interception', E_c), throughfall (*Thro*: $P - E_c$), surface runoff (R), potential groundwater recharge (drainage from soil base at 3 m) (D), near-surface soil moisture content (0–0.1 m; $\Xi_{0-0.1m}$) and total profile soil moisture content (0–3 m; Ξ_{0-3m}). The sum of E_c, E_s and T will be referred to as evapotranspiration, ET.

JULES includes a process-based photosynthesis scheme, enabling it to represent the bio-physical response of vegetated surfaces to climate change. A full description of the scheme, including the mechanism by which it accounts for variation in CO_2 is given in Clark et al. (2011). The following section summarises the key processes.

The leaf-level stomatal conductance g_s is coupled to the rate of photosynthesis via the CO_2 diffusion equation:

$$A = g_s(C_c - C_i)/1.6 \tag{1}$$

where C_c and C_i are the leaf surface and internal concentrations of CO_2, respectively.

JULES represents photosynthesis as the minimum of three regimes: (i) Rubisco-limited rate; (ii) light-limited rate; and (iii) rate of transport of photosynthetic products. Each regime is affected by environmental conditions (Collatz et al., 1991). Leaf photosynthesis (A) is then derived by scaling maximum possible photosynthesis A_p with a metric of available root-zone soil moisture content (β):

$$A = A_p\beta \tag{2}$$

The three limiting rates of photosynthesis and the CO_2 diffusion equation include a number of plant-specific parameters. In order to account for these variations, JULES categorises vegetation cover as a combination of five Plant Functional Types (PFTs): broad leaf trees, needle leaf trees, C3 grass, C4 grass and shrubs.

2.3. JULES model sensitivity runs

A number of model perturbations were conducted to explore the effects of CO_2 fertilisation and 'blanket' land use change:

2.3.1. Effects of CO_2 fertilisation

in addition to the runs described in Section 2.2, JULES was also run with the driving data from the 3 ensemble members with *future* climate but in this case with *present* climate CO_2 concentrations. These runs helped explore the separate effects of changes in meteorology and CO_2 increase (to assess the vegetation's response to CO_2 fertilisation) on the West African water balance, in particular the partitioning of soil moisture to plants (via root water uptake and then transpiration) and to potential groundwater recharge.

2.3.2. Effects of land use change

to examine the controls on the water balance exerted by vegetation type, JULES was run with the entire land area covered with a single vegetation type (as represented by different PFTs), either broadleaf trees or C4 grass (the latter to represent crops such as maize and sorghum), using just one of the present climate ensemble members with present CO_2 concentrations. These runs were to provide a

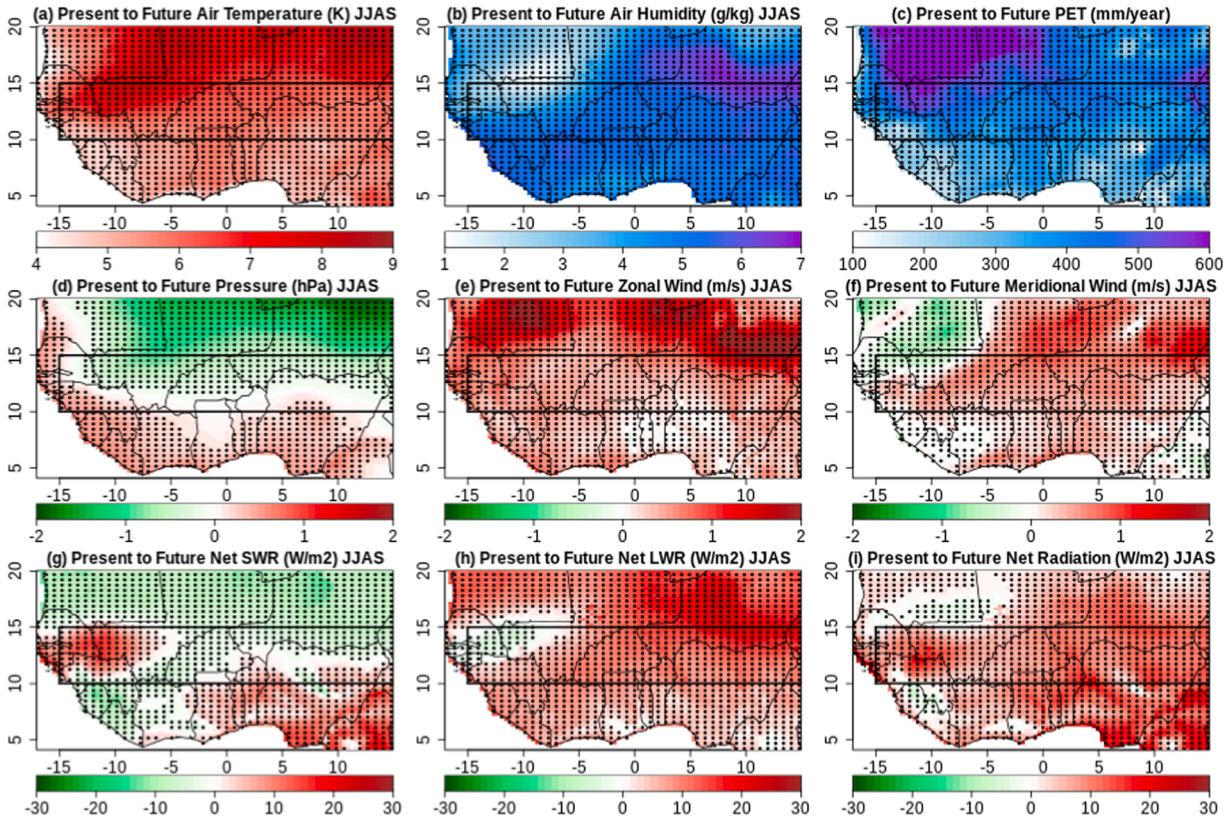

Fig. 3. Absolute changes in UPSCALE multi-year summer (JJAS) means between present (~ year 2000) and future (RCP8.5, ~ year 2100) climate: (a) 2 m air temperature, (b) 2 m specific humidity, (c) potential evapotranspiration (*PET*, note this is based on annual mean values), (d) surface atmospheric pressure, (e) 10 m zonal wind, (f) 10 m meridional wind, (g) surface net shortwave radiation, (h) surface net longwave radiation, (i) surface net total radiation. The black rectangle shows the approximate location of the Sahel. Stippling shows where the changes are 95% significant, according to t-tests.

general picture of the effects of deforestation (transition from trees to mixed vegetation) and intensification of agriculture (transition from the actual mixed vegetation to crops) on the terrestrial water balance.

2.4. Presentation and statistical exploration of model outputs

To examine the change in the meteorological conditions of West Africa, maps were plotted of the changes from present to future climate in the multi-year mean summer (JJAS) UPSCALE temperature and atmospheric variables relating to large-scale circulation. The spatial changes in the monsoon are presented by plotting the absolute increases in the multi-year mean rainfall and the amount of intense rain (P_{high}: $P > 16$ mm/day was chosen as a representative value). Next, the changes in the water balance predicted by JULES were examined by plotting the absolute increases in the multi-year mean water balance components.

In each case, t-tests were used to determine where the changes are 95% statistically significant. For the differences between climate values for two (sets of) model runs (whether directly from UPSCALE or from the JULES outputs driven by UPSCALE):

$$t = \left(\underline{run_1} - \underline{run_2}\right) \Big/ \sqrt{\left(\frac{\sigma^2_{run1}}{N_{run1}} + \frac{\sigma^2_{run2}}{N_{run2}}\right)} \tag{3}$$

here σ is the standard deviation and N the number of years that are available for a particular run, or sets of runs. When comparing the future and present climate model runs, N_{run1} and N_{run2} are 81 (3 × 27 years) and 135 (5 × 27 years), respectively, whereas when comparing the future climate runs with future or present CO_2, $N_{run1} = N_{run2} = 81$, and when comparing the results from different vegetation coverage both equal 27 (i.e., one present climate ensemble only is used to drive JULES). The differences between runs are 95% significant if $t > 2$ (or $t < -2$).

The change in seasonality of the water balance between the present and future climate is also examined by focussing on the region delineated by 5 W to 5 E and 4–21 N, to provide a zonally averaged transect through the Savanna and Sahel climate zones. This transect is used to present the multi-year mean changes in temperature and large-scale circulation, and absolute increases in rainfall and water budgets by latitude and month, to examine the progression of the monsoon, and determine its spatial and temporal changes.

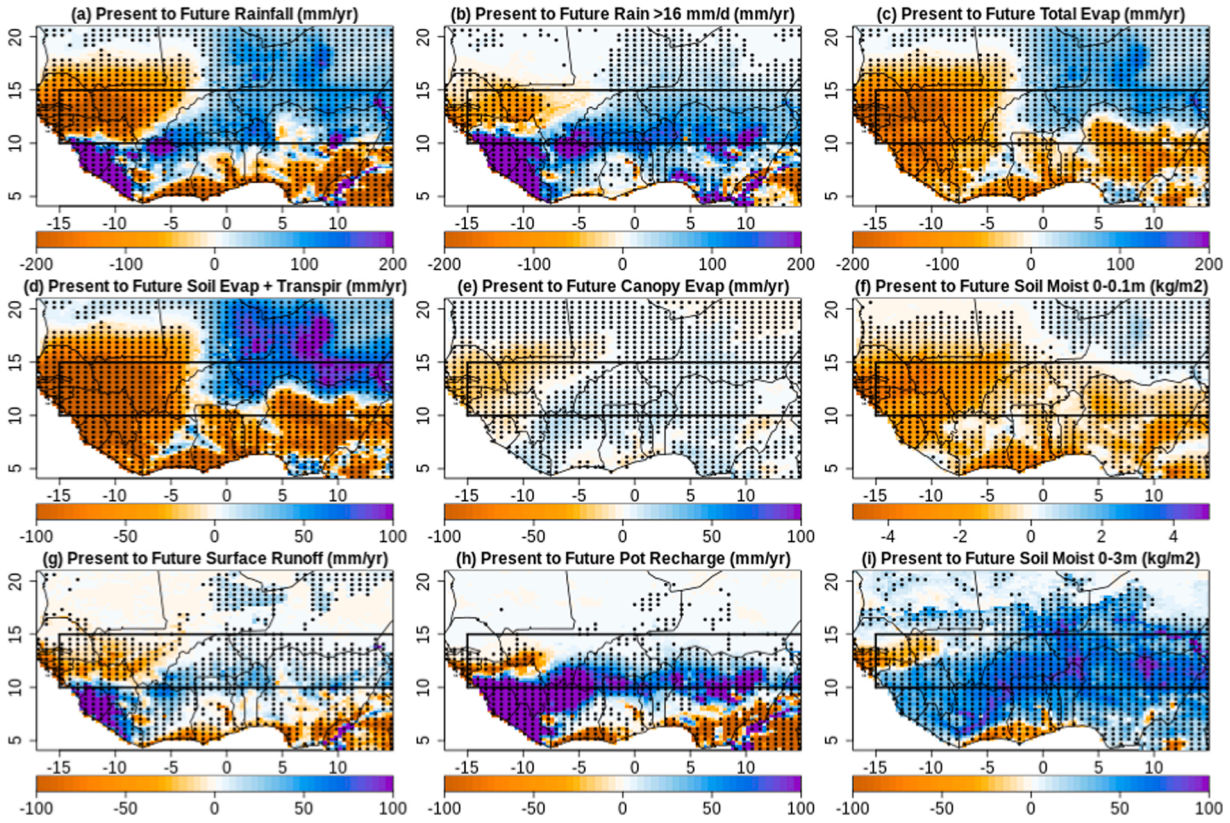

Fig. 4. Absolute changes, calculated from annual multi-year means from present (~ year 2000) to future (RCP8.5 ~ year 2100) climate, in (a) total rainfall from UPSCALE, P (b) high intensity rainfall, P_{high} ($P > 16$ mm/day) from UPSCALE, as well as results generated by JULES (driven by UPSCALE meteorology) for (c) total evapotranspiration, ET (i.e., including interception), (d) evaporation from bare soil plus transpiration from the plants ($E_s + T$; JULES calls this 'soil evaporation', i.e., originating from soil pores and roots), (e) evaporation from the canopy (interception evaporation, E_c), (f) top layer soil moisture (0–0.1 m), $\Xi_{0-0.1m}$, (g) surface runoff, R, (h) potential groundwater recharge, D (called sub-surface runoff in JULES), (i) total column soil moisture content (0–3 m), Ξ_{0-3m}. The black rectangle shows the approximate location of the Sahel. Stippling shows where the changes are 95% significant, according to t-tests.

This central region is further divided into four sub-regions that are largely composed of: southern Ghana (7–9 N), northern Ghana (9–11 N), southern Burkina Faso (11–13 N) and northern Burkina Faso (13–15 N). Although the results for these sub-regions also contain data for other countries (e.g., Benin, Togo, Mali etc.), we refer to them via the names mentioned above. The water balance components and their statistics were calculated within these sub-regions and within two sub-regions on either side: west Sahel (WS: 15–5 W, 10–15 N) and east Sahel (ES: 5–15 E, 10–15 N). Fig. 1 shows the locations of the sub-regions.

Finally, to examine in more detail the range of summer (JJAS) monthly P values, and the dependence of ET, R and D on monthly P, the northern Ghana and southern Burkina Faso sub-regions were selected, as there is limited variation in rainfall patterns and vegetation and soil. The modelled P and relevant water balance output values from each grid box in these regions for each summer month in all years were divided into 20 bins of equal numbers of grid box months according to rainfall amount. Hence, the bins range from the 5% driest months to the 5% wettest months, to accurately represent the rainfall distribution; in each bin the means and standard deviations were calculated for the rainfall and other variables. Then ET, E_c, $Thro$, R and D (all expressed as percentage of monthly rain) were plotted against monthly P, for present and future climates (and future climate with present CO_2 concentrations; see Section 2.3 for more detail).

3. Results and discussion

3.1. UPSCALE ensemble outputs and JULES water balance outputs driven with UPSCALE data

3.1.1. Present to future changes; spatial distributions across the entire West-African domain

The UPSCALE multi-year mean summer (JJAS) near-surface meteorological conditions from present (1985–2011) to future (2085–2111) predict air temperature increases of 4–9 °C, with the greatest increases over the Sahara (Fig. 3a), a zone of decreased atmospheric air pressures (Fig. 3d); we find increased air pressures in the coastal zones. With predicted increases in the meridional gradients over the Sahel (here defined as 10–15 N), the enhanced Saharan heat low perturbs large-scale summer circulation under

Table 1
Multi-year mean annual changes (expressed as a percentage) in total rainfall, P (from UPSCALE), canopy evaporation, E_c (see also Fig. 4e), evapotranspiration, ET (see also Fig. 4c), surface runoff R (see also Fig. 4g), potential recharge (drainage from soil base at 3 m), D (see also Fig. 4h), near-surface soil moisture content, $\Xi_{0-0.1m}$ (see also Fig. 4f) and total profile soil moisture content, Ξ_{0-3m} (see also Fig. 4i), from the JULES runs driven by UPSCALE atmospheric variables (see Sections 2.2 and 2.3) from present climate to future climate with present CO_2 concentration [*italics*] and from present climate to future climate with future CO_2 concentration [**bold**], in the six sub-regions (see Fig. 1, black boxes).

Sub-region Flux or store	W Sahel	S Ghana	N Ghana	S Burkina Faso	N Burkina Faso	E Sahel
P	**-13.5%**	**-1.2%**	**+ 6.9%**	**+ 8.9%**	**+ 7.7%**	**+ 12.2%**
E_c	*-9.2%*	*+ 3.0%*	*+ 6.3%*	*+ 6.7%*	*+ 2.8%*	*+ 6.0%*
	-9.2%	**+ 3.7%**	**+ 7.1%**	**+ 6.7%**	**+ 2.8%**	**+ 7.5%**
ET	*-13.1%*	*+ 2.0%*	*+ 6.0%*	*+ 6.5%*	*+ 7.1%*	*+ 10.0%*
	-19.3%	**-2.3%**	**-1.8%**	**+ 2.3%**	**+ 6.3%**	**+ 5.5%**
R	*-13.5%*	*-12.2%*	*+ 13.2%*	*+ 28.6%*	*0.0%*	*+ 26.1%*
	-10.4%	**-4.1%**	**+ 26.3%**	**+ 42.9%**	**0.0%**	**+ 34.8%**
D	*-15.3%*	*-52.9%*	*+ 11.8%*	*+ 100.0%*	–	*+ 30.0%*
	+ 11.5%	**+ 13.7%**	**+ 145.1%**	**+ 333.3%**		**+ 110.0%**
$\Xi_{0-0.1m}$	*-21.4%*	*-9.5%*	*-5.0%*	*-6.7%*	*-14.3%*	*-11.1%*
	-21.4%	**-4.8%**	**-5.0%**	**-6.7%**	**-14.3%**	**0.0%**
Ξ_{0-3m}	*-2.7%*	*-4.7%*	*-0.7%*	*+ 1.3%*	*+ 2.8%*	*+ 3.7%*
	+ 2.5%	**+ 6.2%**	**+ 9.2%**	**+ 11.2%**	**+ 11.4%**	**+ 13.9%**

future climate with increased monsoon winds. The model runs also indicate zonal winds are increased, particularly over the Sahara, while the meridional winds are increased across much of West Africa, particularly over the eastern Sahel, but reduced over the western Sahel (Fig. 3e–f). These findings fit with those of Cook and Vizy (2015) who used three reanalyses of 1.5° resolution (ERA-Interim, NCEP-2 and MERRA) and two observational datasets of 0.5° (CRU and GHCN) for 1979–2012 to show that the Sahara temperature has increased 2–4 times faster than the tropical mean, strengthening the summertime heat low and African easterly jet, while weakening the wintertime anticyclone and low-level Harmattan winds.

Near-surface specific atmospheric humidity (Fig. 3b) is also projected to increase, consistent with higher temperatures and stronger monsoon winds carrying more moisture originating from the Gulf of Guinea. For future climates, net shortwave radiation (Fig. 3g) is reduced over most of the Sahel indicating that cloud coverage has increased (surface albedo was kept constant between present and future). However, net shortwave radiation has increased in parts of the west (between 10 and 12 N) and in the coastal region around the Gulf of Guinea, which has increased winds from the north bringing in drier air masses with fewer clouds. This is also apparent from the reductions in rainfall for future climate conditions (see Fig. 4a). Net longwave radiation (Fig. 3h) is increased over most of the area except for a small area in the west, coinciding with the area of increased net shortwave radiation. Future longwave radiation will be increased as a result of the higher air temperatures, causing increased values of downwelling radiation from the atmosphere and clouds (based on Stefan Boltzmann's law: $L_{\downarrow} = \varepsilon_a \sigma T_a^4$; with ε_a the atmospheric emissivity and σ the Stefan Boltzmann constant). Note, however, that the increase in downwelling longwave radiation will be countered in part by increased upwelling longwave radiation from the land surface, caused by reductions in total *actual ET* (see Fig. 4c). Atmospheric emissivity, and hence net longwave radiation, also depends on cloud cover, type of clouds, air temperature and humidity, so the changes in these variables will have moderated the extent of the increase in net longwave radiation. Although we are not presenting a figure of cloud-cover, Fig. 4a, showing the changes in precipitation between present and future climate, implies that changes in cloud-cover will be variable across the region. Total net radiation, i.e., net shortwave plus net longwave radiation, is generally increased (Fig. 3i), as the increase in net longwave radiation is greater than the decrease in net shortwave radiation.

Values for *PET* (see Section 2.1 for details on its calculation) are also predicted to increase under future climates (only positive changes are shown in Fig. 3c), largely as a result of increased temperatures (Fig. 3a) and net radiation (Fig. 3i). Increased *PET* means atmospheric water demand will be greater in the future but present-to-future changes in *actual ET* (see Fig. 4c, and Table 1) will be modulated by changes in the availability of soil water, and by changes in atmospheric CO_2 concentration (via the CO_2 fertilisation effect); both affect T, via root water uptake and plant physiological feedbacks that dictate the degree of stomatal opening.

Future annual P (Fig. 4a) is increased in the central, southwest and northeast regions of West Africa (+ 12.2% in east Sahel, + 6.9% in northern Ghana and + 8.9% in southern Burkina Faso sub-regions, Table 1), but reduced in the south and west (− 13.5% in west Sahel), a pattern consistent with the change in summer large-scale circulation, due to the enhanced heat low (see Fig. 3d–f). Kamga et al. (2005) found that increased atmospheric moisture and stronger meridional winds would lead to a wetter Sahel in the late 21st century; our findings show a wetter eastern Sahel but a drier western Sahel. The change in the spatial pattern of rainfall presented in Fig. 4a is similar to the multi-model CMIP5 mean described by Roehrig et al. (2013) and Diallo et al. (2016), and also to the predictions of Gaetani et al. (2020).

The increases in P_{high} (Fig. 4b) are greater than those for total P, over large areas, and heavy rain is even increased for many areas in the south where the total is reduced, showing that rainfall becomes more intense under future climatic conditions. Table 2 shows that in the future, P_{high} is a greater fraction of the total P in all six sub-regions, with increases ranging between 4% and 11% (row 1 in Table 2) compared to the present climate. Sylla et al. (2015) and Fitzpatrick et al. (2020) also predict more intense rainfall events, due to stronger moisture convergence in the future.

Total ET (which includes interception evaporation), as well as the sum of E_s and T (what JULES calls the evaporation from the soil

Table 2
Multi-year absolute mean annual fractions (expressed as a percentage of total rainfall P from UPSCALE), in the six sub-regions (see Fig. 1, black boxes) for: high intensity rainfall, P_{high} ($P > 16$ mm/day), and the water balance fluxes obtained from the JULES runs described in Sections 2.2 and 2.3. The symbols are as defined in the caption of Table 1. JULES was driven with present climate data [plain text], future climate with present CO_2 concentration [*italics*] and future climate with future CO_2 concentration [**bold**].

Sub-region Flux	W Sahel	S Ghana	N Ghana	S Burkina Faso	N Burkina Faso	E Sahel
P_{high}/P	34.8%	13.7%	19.7%	20.8%	16.0%	16.0%
	40.2%	**17.4%**	**28.4%**	**29.5%**	**21.5%**	**27.1%**
E_c/P	8.6%	11.9%	10.9%	12.1%	14.4%	10.7%
	9.1%	*12.4%*	*10.8%*	*11.9%*	*13.7%*	*10.1%*
	9.1%	**12.5%**	**10.9%**	**11.9%**	**13.7%**	**10.3%**
ET/P	75.0%	89.0%	88.9%	94.6%	100.0%	92.8%
	75.3%	*91.9%*	*88.2%*	*92.6%*	*99.4%*	*91.0%*
	69.9%	**88.1%**	**81.7%**	**89.0%**	**98.7%**	**87.3%**
R/P	9.5%	6.5%	6.6%	4.1%	1.6%	3.7%
	9.5%	*5.8%*	*7.0%*	*4.8%*	*1.5%*	*4.1%*
	9.9%	**6.3%**	**7.8%**	**5.4%**	**1.5%**	**4.4%**
D/P	15.6%	4.5%	4.4%	1.4%	0.0%	4.8%
	15.3%	*2.1%*	*4.6%*	*2.6%*	*0.6%*	*5.6%*
	20.1%	**5.2%**	**10.1%**	**5.6%**	**0.8%**	**9.0%**

compartment), is predicted to decrease across large areas in the west and south of West Africa (Fig. 4c), despite the increased P and PET values (Fig. 3c). Under future climate conditions, ET is projected to decrease considerably for west Sahel (by nearly 20%) and somewhat for northern and southern Ghana, whereas it increases between 2% and 6% for the other regions. Within all six sub-regions ET/P is reduced, by 1–7% (see Table 2). $E_s + T$ (see Fig. 4d) is reduced over large areas, whereas E_c (Fig. 4e) is generally slightly increased due to the greater rainfall and increased PET, but not in the eastern Sahel, where rainfall is reduced. The decreased evaporation from the soil compartment is most likely mainly due to reduced T, as this is generally the largest component in ET. The near-surface soil moisture contents ($\Xi_{0-0.1m}$; Fig. 4f) are reduced over most of West Africa and in most sub-regions (Table 1, row 3), in particular for the west Sahel where rainfall is decreased. Also, in the future, $E_s + T$ (which is predominantly composed of T) is reduced despite the higher Ξ_{0-3m} values (Fig. 4i and Table 1), indicating that reduced T is not caused by increased plant water stress, as this would occur if soil moisture contents were reduced. Rather, reduced transpiration in the future is caused by the concurrent climatic feedbacks (relating to physical variables as well as increased CO_2 concentration) affecting photosynthesis and lowering stomatal conductance (see e.g., Kirschbaum and McMillan, 2018).

Surface runoff, R, and potential groundwater recharge, D, (Fig. 4g–h) overall show modest to relatively large increases (note that these changes are not statistically significant over the northern parts of the West African domain). The projected changes in R vary between a decrease of 10% (West Sahel) to an increase of $> 40\%$ (S Burkina Faso), mainly because of the larger amount of rain falling during heavy events (see Table 2); this causes increased R, particularly where surfaces are bare or sparsely vegetated. Interestingly, D is predicted to increase in all regions (apart from northern Burkina Faso, where the model simulates $D = 0$ for present climate), and for some regions quite dramatically, e.g., northern Ghana (145%), south Burkina Faso (333%) and east Sahel (110%). This is largely related to an increase in Ξ_{0-3m} (Fig. 4i) that goes up by between 2.5% and 14% for future climate conditions (Table 1), as a result of increased (P-ET) values, demonstrating a shift in the water stored in the soil between present and future climate, mainly as a result of reduced root water uptake. Increased values of Ξ_{0-3m} cause soil hydraulic conductivity to increase, which in turn increases potential groundwater recharge.

However, values of R/P barely change in most sub-regions (by about $-$ 2.5% maximally, for potential recharge in southern Ghana, row 3, Table 2). In contrast, future D/P increases considerably under future climate conditions (bold numbers in Table 2): whereas under the present climate conditions D takes up anywhere between 0% and 16% of total rainfall, in the future this is 1–20%, with a doubling from $\sim$ 5 to $\sim$ 10% in northern Ghana and east Sahel.

Part of the shift in water balance is caused by a greater proportion of the increased rainfall passing through the canopy as throughfall (*Thro*, see also Fig. 6a–b), rather than evaporating from there (*Ec*), and reaching the soil surface where it then either runs off or infiltrates into the soil. The values of Ec/P are slightly reduced over Burkina Faso and east Sahel in Table 2. Note that ET is also inhibited during rain, due to reduced solar radiation and increased humidity, which allows more of the water to infiltrate the soil. Future rainfall amounts show moderate changes of between $-$ 13.5% (west Sahel) and + 12.2% (east Sahel) in Table 1.

3.1.2. Present to future changes; effects of plant physiological response and vegetation cover

For improved understanding of the future changes in water balance, the separate effects of the physical meteorological driving variables and the plant physiological response to increased CO_2 were examined by using the JULES runs with future climate, but with CO_2 concentrations kept at present levels (see Section 2.3). The results are presented in Fig. 5 and Tables 1 and 2. Also, the influence of vegetation cover on the terrestrial water balance was considered (see Tables 3 and 4).

With just the changes in meteorology (the climate effect - Fig. 5; left plots), total ET changes (Fig. 5d) are largely resulting from the changes in P, as illustrated by a very similar spatial patterns of rainfall increase (Fig. 4a). Changes in Ξ_{0-3m} (Fig. 5g) also roughly reflect the rainfall pattern, while R and D (Fig. 5a, j) show increases well inland between 9 and 13 N where the greatest increases in heavy

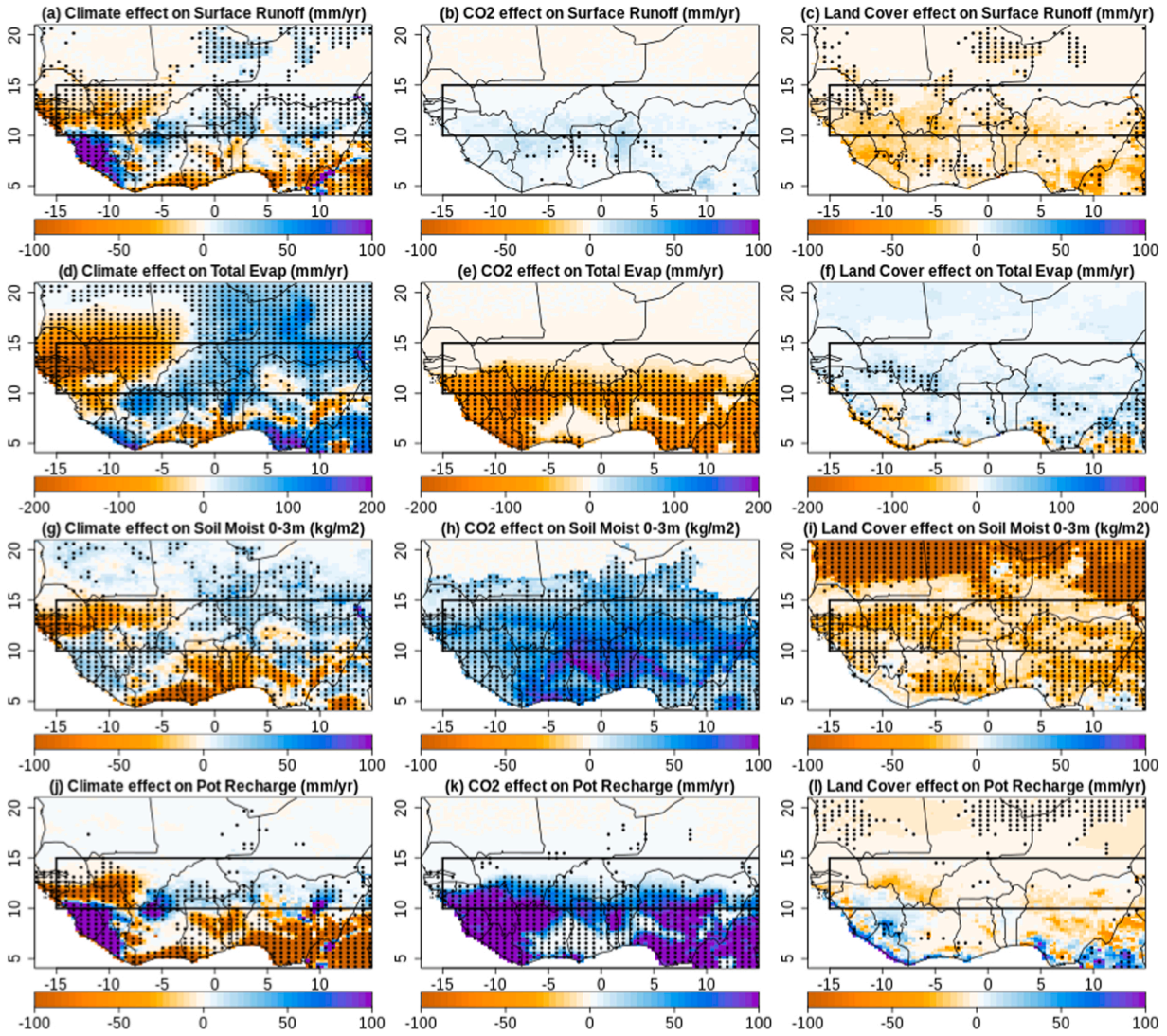

Fig. 5. Absolute changes in annual multi-year mean surface runoff, R (first row), total evapotranspiration, ET (second row), total column soil moisture, Ξ_{0-3m} (third row), and potential recharge, D (fourth row) with: the climate effect – change in meteorology from present to future climate only, i.e. CO_2 remains at present concentrations and vegetation cover (mixed) is taken from maps (first column); the CO_2 effect – increase in CO_2 concentration only, using future meteorology and mixed vegetation (second column); the land cover effect – change in vegetation coverage from mixed to C4 grass (crops such as sorghum and maize), these plots represent one UPSCALE ensemble member with present climate and CO_2 (third column). The black rectangle shows the approximate location of the Sahel. Stippling shows where the changes are 95% significant, according to t-tests.

rainfall ($>$ 16 mm/day) occur (Fig. 4b), whereas regions to the west and south have reduced potential recharge. In south Burkina Faso and east Sahel ET does not increase as much as rainfall, leading to increased Ξ_{0-3m}, between 1% and 4% (Table 1), and to slightly increased R/P values compared to present climate, $\sim$ 0.4%, and D, $\sim$ 0.7% (Table 2). The increases in Ξ_{0-3m} and D, despite the increased PET (see Fig. 3c), are driven by increased rainfall.

With just the increase in CO_2, for future climatic conditions (the CO_2 effect - Fig. 5; middle), $E_s + T$, and hence total ET (Fig. 5e), is reduced across West Africa, which confirms that reduced total ET is largely due to the vegetation CO_2 response. Ξ_{0-3m}, R and D (Fig. 5h, b, k) are increased across West Africa because less water is removed from the soil by plant roots, as stomatal opening and therefore transpiration is reduced. These observations hold in all sub-regions (Tables 1 and 2), with D/P further increased by between 3% and 5% of the total rainfall.

Comparing mixed vegetation to uniform C4 grass (representing crops such as sorghum and maize), the land cover effect, water balance differences are subtle with slight increases in total ET across most of West Africa (Fig. 5f) and mostly small reductions in Ξ_{0-3m}, R and D (Fig. 5i, c, l). The exception is the Sahara, where soil moisture reductions are large under the previously bare ground, and the soil moisture changes are generally more significant. Evaporation is increased by 1–2% in the sub-regions, reducing Ξ_{0-3m} content by

Table 3
Multi-year mean annual changes (expressed as a percentage) due to changed vegetation cover, for the water balance fluxes and soil moisture stores obtained from the JULES runs as described in Section 2.3. The symbols are as defined in the caption of Table 1. Results are presented for a change from mixed vegetation to uniform broadleaf trees [*italics*], and from mixed vegetation to uniform C4 grass (representing crops such as sorghum and maize) [**bold**] . For these runs only one *present* climate ensemble member was used to drive JULES ($N = 27$). Data are presented for the six sub-regions presented in Fig. 1.

Sub-region Flux or store	W Sahel	S Ghana	N Ghana	S Burkina Faso	N Burkina Faso	E Sahel
E_c	*+ 20.7%*	*+ 18.7%*	*+ 16.0%*	*+ 20.0%*	*+ 38.0%*	*+ 32.8%*
	+ 11.5%	**+ 8.2%**	**+ 5.6%**	**+ 9.5%**	**+ 26.8%**	**+ 20.9%**
ET	*+ 2.5%*	*+ 0.6%*	*-0.1%*	*-0.1%*	*+ 0.2%*	*+ 1.2%*
	+ 2.0%	**+ 1.0%**	**+ 1.4%**	**+ 1.5%**	**+ 1.0%**	**+ 1.6%**
R	*-1.1%*	*+ 2.9%*	*+ 5.6%*	*+ 2.9%*	*0.0%*	*-4.3%*
	-10.5%	**-10.0%**	**-13.9%**	**-22.9%**	**-25.0%**	**-17.4%**
D	*-10.9%*	*-14.6%*	*-2.2%*	*+ 9.1%*	*0.0%*	*-17.2%*
	-2.6%	**-2.1%**	**-4.3%**	**-18.2%**	**-100.0%**	**-13.8%**
$\Xi_{0-0.1m}$	*+ 28.6%*	*+ 20.0%*	*+ 15.0%*	*+ 26.7%*	*+ 57.1%*	*+ 33.3%*
	+ 7.1%	**+ 5.0%**	**0.0%**	**+ 6.7%**	**+ 28.6%**	**+ 11.1%**
Ξ_{0-3m}	*-0.8%*	*+ 3.0%*	*+ 2.1%*	*+ 2.9%*	*+ 4.3%*	*-0.9%*
	-3.0%	**-2.4%**	**-1.7%**	**-3.4%**	**-3.8%**	**-5.1%**

Table 4
Multi-year absolute mean annual fractions (expressed as a percentage of total rainfall *P* from UPSCALE) for the water balance fluxes obtained from the JULES runs as described in Section 2.3, using one present climate ensemble member. The symbols are as defined in the caption of Table 1. Data are shown for mixed vegetation [plain text], uniform broadleaf trees [*italics*] and uniform C4 grass (representing crops such as sorghum and maize) [**bold**].

Sub-region Flux	W Sahel	S Ghana	N Ghana	S Burkina F	N Burkina F	E Sahel
E_c/P	8.6%	12.1%	11.0%	12.3%	14.1%	10.8%
	10.4%	*14.3%*	*12.7%*	*14.8%*	*19.5%*	*14.3%*
	9.6%	**13.1%**	**11.6%**	**13.5%**	**17.9%**	**13.0%**
ET/P	75.1%	89.3%	89.4%	94.5%	99.6%	92.8%
	77.0%	*89.8%*	*89.3%*	*94.4%*	*99.8%*	*93.9%*
	76.6%	**90.2%**	**90.6%**	**95.9%**	**100.6%**	**94.2%**
R/P	9.4%	6.3%	6.3%	4.1%	1.6%	3.7%
	9.3%	*6.5%*	*6.7%*	*4.2%*	*1.6%*	*3.5%*
	8.4%	**5.7%**	**5.4%**	**3.2%**	**1.2%**	**3.0%**
D/P	15.5%	4.3%	4.0%	1.3%	0.2%	4.7%
	13.8%	*3.7%*	*4.0%*	*1.4%*	*0.2%*	*3.9%*
	15.1%	**4.2%**	**3.9%**	**1.1%**	**0.0%**	**4.0%**

2–5%, though $\Xi_{0-0.1m}$ is increased (apart from northern Ghana), by between 5% and 29% (Table 3).

R is reduced by ~ 1% when expressed as fraction of the rainfall, and potential recharge by < 1% (Table 4), when the land cover is changed from mixed vegetation to C4 grass. The changes, and the absolute values of the flux partitioning in Table 4, correspond well with those shown in Table 2 (for present conditions), even though only one present climate ensemble member was used to produce the results in Table 4. This indicates the robustness of the individual UPSCALE ensemble members. These changes show greater water uptake by the C4 grass (representing crops). Going from mixed vegetation to uniform broadleaf trees results in: little change in total *ET* in the central sub-regions, despite the increase in E_c and Ξ_{0-3m} (by 2–4%); slightly increased *R;* and only slight changes in *D*.

3.1.3. Spatiotemporal dependencies of the water balance fluxes on rainfall amount and frequency

The dependence of the water balance flux partitioning on rainfall amount and frequency is examined more closely by taking values for each individual summer month for each grid square in the sub-regions of northern Ghana and southern Burkina Faso and arranging these by amount of rainfall. Fig. 6a–b shows that *Thro* increases from ~ 80% of *P* in the driest summer months to ~ 96% in the wettest months. This indicates that proportionally less water evaporates from the canopy during the wettest months, as is also apparent from the decrease in E_c (lowest line in these plots). The fractions allocated to *Thro* only depend on the amount of rain, with the same relationship for present and future climate, so allocation to *Thro* is predicted to increase slightly in the future as rainfall increases. With an increase in monthly rainfall, the fraction of *ET* goes from an average of 100% of the monthly rainfall (or more for individual gridcells, with the additional water coming from the water already stored in the soil) to only 20–30%, partly due to the suppression of *ET* during rainfall and during conditions of high relative humidity. Contributions of monthly rainfall to *R* and *D* are near zero in the driest months but can be greater than 25% and 45% of the rainfall, respectively, in the wettest months (Fig. 6c–f).

From present (blue lines in Fig. 6) to future meteorological conditions (red lines for present CO_2 and black lines for future CO_2), both the mean values and the standard deviations of the highest monthly rainfall values increase (rainfall ranges also shown at the top of Fig. 6c–d); this is important since Vellinga et al. (2016) found that most inter-annual variability is from changes in organised heavy

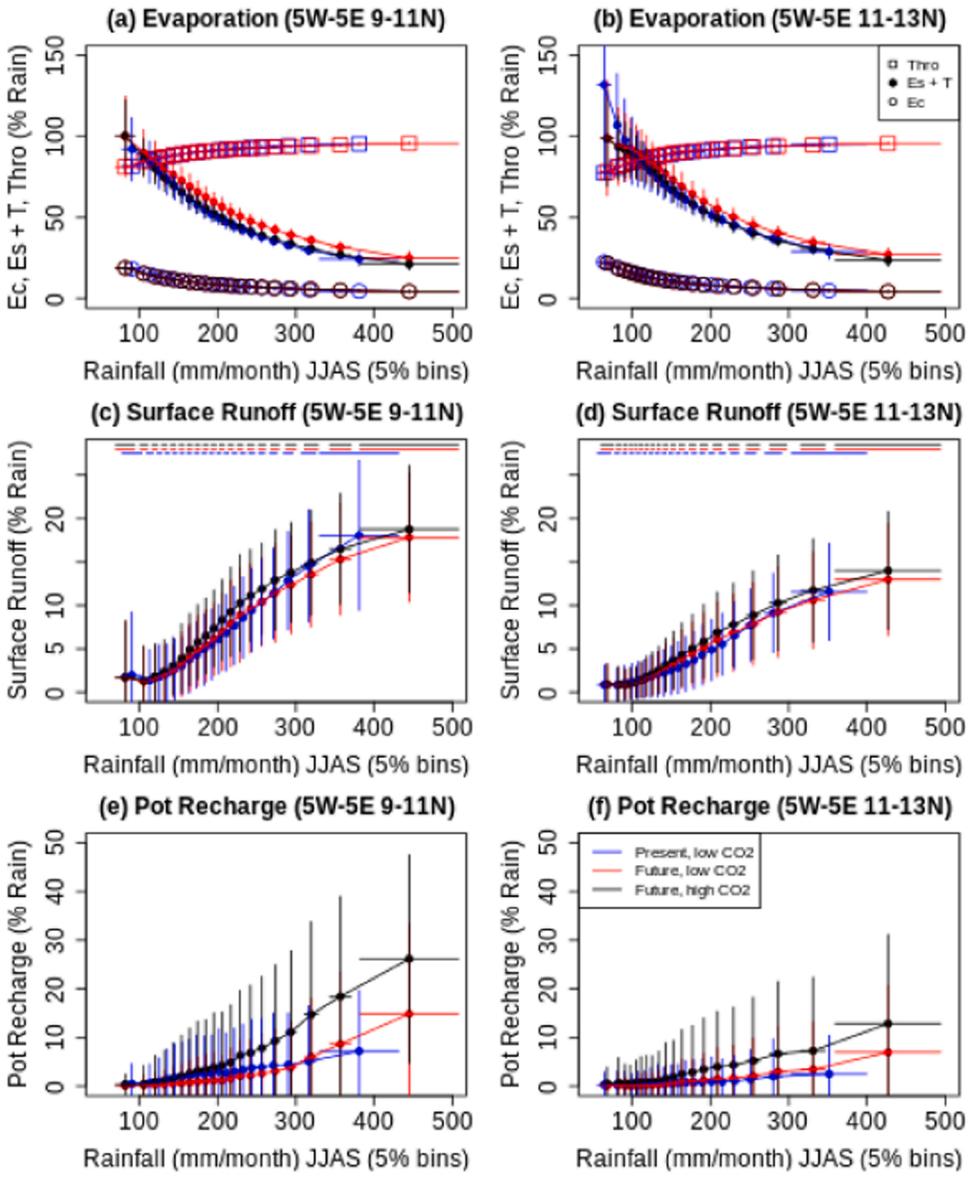

Fig. 6. (a–b) JULES *Thro* (top lines except at low rainfall), $E_s + T$ (middle set of lines except at low rainfall), and E_c (bottom lines in plots); (c–d) surface runoff, R (with the standard deviations in rainfall also shown at the top of the plots); and (e–f) potential groundwater recharge, D. All fluxes on the y-axes are summer values (JJAS), expressed as percentages of total monthly rainfall, and plotted vs monthly rainfall, together with their mean and standard deviation, from each summer month and 25 km grid square. Rainfall is presented in twenty 5% bins from the month-grid square combinations from the 5% with the least rain to the 5% with the most rain. Plots are for present climate and CO_2 (blue), future climate with present CO_2 (red), and future climate with future CO_2 (black), in the northern Ghana (5 W to 5 E, 9–11 N, left) and southern Burkina Faso (5 W to 5 E, 11–13 N, right) sub-regions.

rainfall events. If CO_2 concentration remains unchanged (red lines), the higher temperatures (and resulting *PET*) lead to greater *ET*, although because of the increase in the highest monthly rainfalls, *ET* represents a smaller portion of the rain.

When going from present to future meteorology at present CO_2 concentrations (red lines), the fraction allocated to R (Fig. 6c–d) is slightly increased in low rainfall months, but reduced in high rainfall months, while the contribution to D (Fig. 6e–f) is slightly reduced in low rainfall months but increased in high rainfall months, although the changes are small compared to the increase in *ET* fraction. At future CO_2 combined with future meteorological conditions (black lines), the fraction of monthly rainfall allocated to D is generally increased, and the ratio R/P slightly increased, as T (and hence overall *ET*) is reduced due to the plant response to increased CO_2 (causing stomata to close).

It is expected that high rainfall leads to increased D because of higher Ξ_{0-3m} (Fig. 4i). Fig. 6e–f shows that this effect is amplified by greater allocation of P to D during high rainfall months. Under future climate and increased CO_2 conditions this is even more evident,

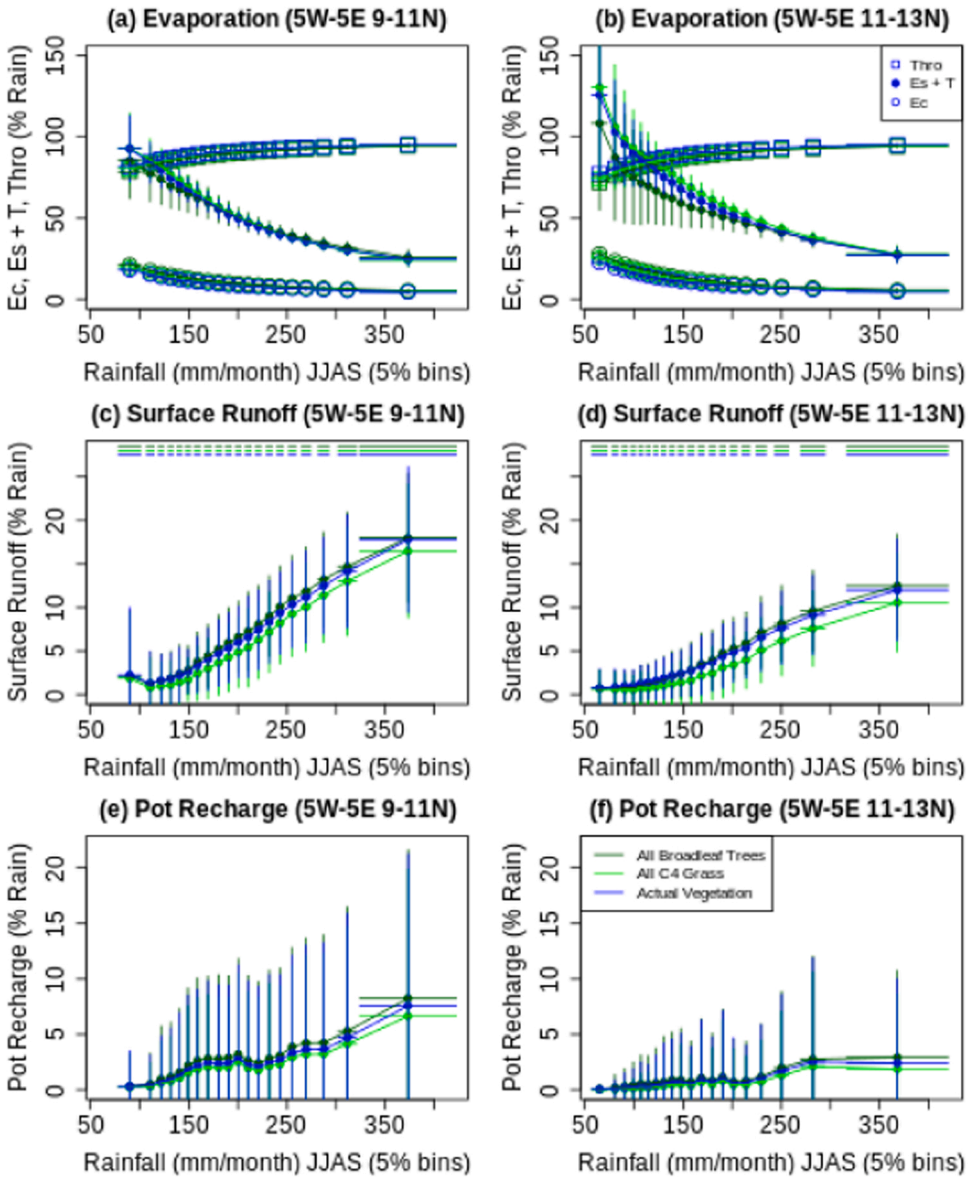

Fig. 7. (a–b) JULES *Thro* (top lines except at low rainfall), $E_s + T$ (middle set of lines except at low rainfall), and E_c (bottom lines in plots), plotted vs monthly rainfall; (c-d) surface runoff, R (with the standard deviations in rainfall also shown at the top of the plots); and (e–f) potential recharge, D, plotted vs monthly rainfall. All fluxes on the y-axes are summer values (JJAS), expressed as percentages of total monthly rainfall, together with their mean and standard deviation, from each summer month and 25 km grid square. Rainfall is presented in twenty 5% bins from the month-grid square combinations from the 5% with least rain to the 5% with the most rain, using one UPSCALE ensemble member with present climate and CO_2. For actual mixed vegetation coverage (blue), all broadleaf trees (dark green) or all C4 grass (light green, to represent crops such as sorghum and maize), in the northern Ghana (left) and southern Burkina Faso (right) sub-regions.

with high rainfall months associated with significantly greater allocation to D than in present climate. When CO_2 is held at present levels, however, the allocation to D under future meteorological conditions is similar to that under present conditions, unless $P > \sim 350$ mm month^{-1}. This suggests that the main driver of increased allocation of P to D is decreased T, and hence reduced extraction of moisture from the soil column. Any effect of intensification of rainfall between present and future climate on E_c is not evident (Fig. 6a–b), only the total amount of rain. The importance of reduced T for increased D, is not highlighted by many studies on the impact of climate change on groundwater resources, with intensification of rainfall considered the primary driver (Taylor et al., 2013). However, it should be noted that the JULES model does not incorporate the process of focussed recharge in areas where surface runoff concentrates, a process which is likely to become more important for groundwater recharge with rainfall intensification (Jasechko and Taylor, 2015; Cuthbert et al., 2019).

Comparing the sub-regions of northern Ghana (Fig. 6 left column) and southern Burkina Faso (Fig. 6 right column), the

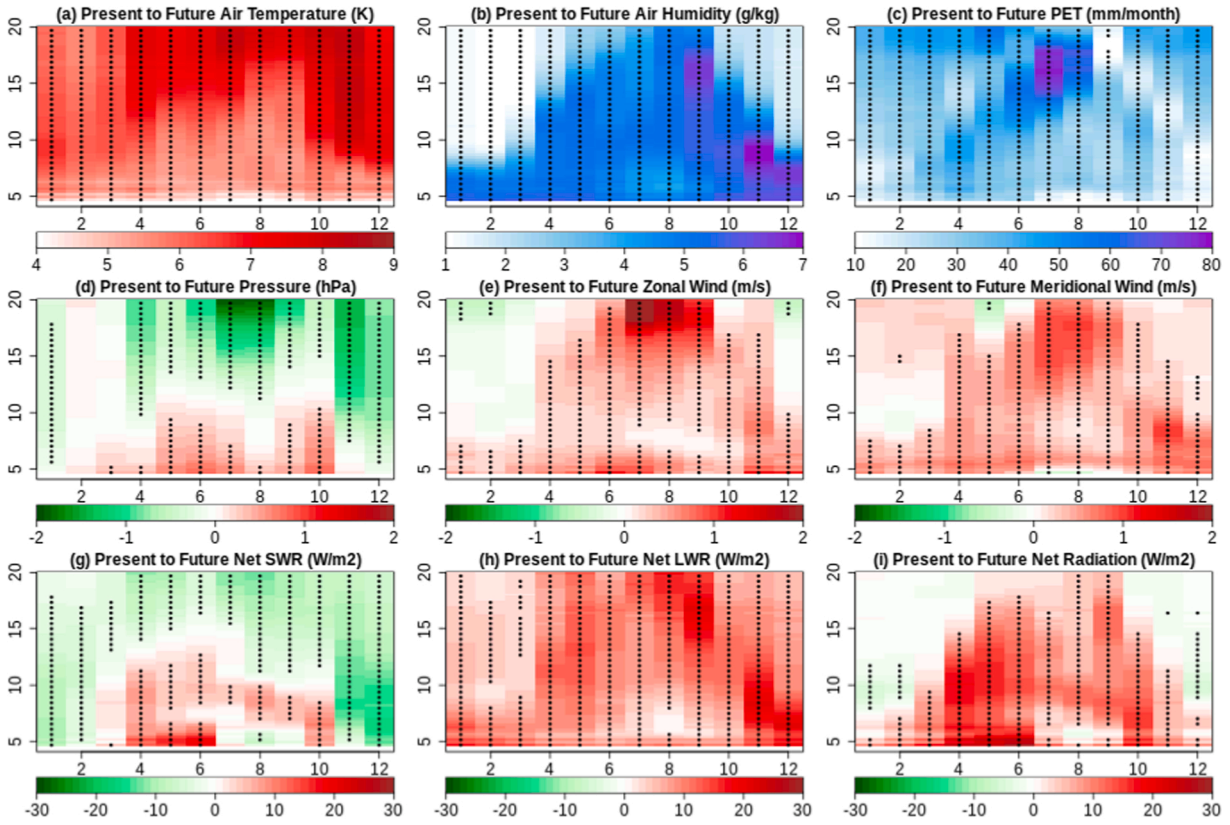

Fig. 8. Absolute monthly (1–12 on x-axis) changes from present (~ year 2000) to future (RCP8.5 ~ year 2100) climate in the multi-year mean seasonal cycle of the UPSCALE driving variables. These are zonal means, between 5 W and 5 E, at different latitudes (y-axis: 5–20 N) for: (a) 2 m air temperature, (b) 2 m specific humidity, (c) potential evapotranspiration, *PET*, (d) surface atmospheric pressure, (e) 10 m zonal wind, (f) 10 m meridional wind, (g) surface net shortwave radiation, (h) surface net longwave radiation, and (i) surface net total radiation. Stippling shows where the changes are 95% significant, according to t-tests.

dependencies on monthly rainfall, climate and CO_2 concentration are similar, but overall the allocation to *ET* is greater, and the allocations to *R* and *D* less, in the hotter climate of Burkina Faso. Table 2 shows the overall mean allocations in these sub-regions.

Similarly, the effects of land cover on the dependency of the monthly water balance components on monthly rainfall are examined, in Fig. 7, by using the JULES runs with uniform vegetation (one of the present climate UPSCALE ensemble members, with present CO_2). Uniform broadleaf tree cover leads to slightly increased proportions of monthly rainfall allocated to E_c (due to the taller canopy, which increases turbulence, and higher leaf area index), reduced *ET* (especially in southern Burkina Faso), and slightly greater *R* and *D* values than for the mixed vegetation coverage (northern Ghana). A simulated land-use change to uniform C4 grass cover also gives slightly increased E_c, though not as much as for the trees, but increased *ET* and slightly lower *D* compared to the mixed coverage, though again these are only minor effects. At high monthly rainfall amounts the *ET/P* ratios converge. Tables 3 and 4 show the overall mean changes in these sub-regions.

3.1.4. Present to future changes; seasonal variations and shifts

Analysis of seasonality focusses on the region delineated by 5 W to 5 E and 4–21 N. Air temperatures are increased throughout the year from present to future climate, with enhanced meridional gradients in temperature and surface pressure from late spring to early autumn (Fig. 8a and d). Many of the variables in Fig. 8 show a northwards progression during spring to give the greatest increases over the north in the summer, followed by a southward retreat in the autumn for humidity, *PET*, and wind. There are reduced values of net shortwave radiation (implying greater cloud cover), for most of the year and latitudes, but increases during the summer months for the southern half (implying less cloud). Net longwave radiation has increased over the entire domain, in particular during autumn and winter, whereas total net radiation is increased particularly in late spring.

Total rainfall is slightly increased in late spring, reduced in early summer, then increased in late summer and autumn (Fig. 9a). In the south, rainfall is reduced over most of the year then increased in autumn, while heavy rain (Fig. 9b) is reduced in June and July between 5 and 7 N but increased particularly in August and September between 9 and 12 N. The pattern of temporal and spatial changes shows that the monsoon occurs later in summer and moves northwards in the future climate. Ibrahim et al. (2014) used simulated rainfall data produced by five regional climate models (under the A1B scenario over two periods: 1971–2000 as reference period and 2021–2050 as projection period) and found that the rainy season onset is projected by all models to be delayed by one week

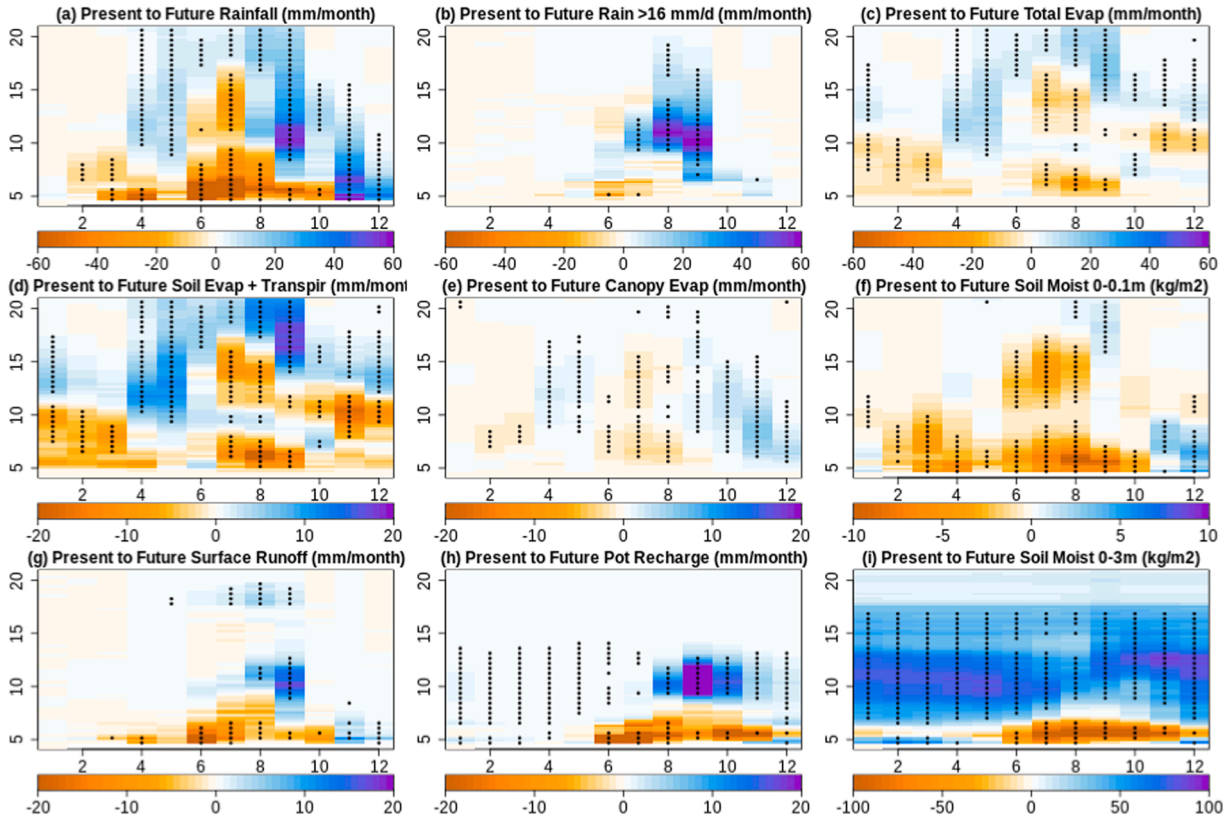

Fig. 9. Absolute changes from present (~ year 2000) to future (RCP8.5 ~ year 2100) climate in JULES multi-year monthly (1–12 on x-axis) hydrological outputs (driven by UPSCALE meteorology). These are zonal means, between 5 W-5E, at different latitudes (y-axis: 5–20 N) for: (a) total rainfall, (b) heavy rain (> 16 mm/day), (c) total evapotranspiration, *ET*, (d) evapotranspiration from soil and plants, $E_s + T$, (e) evaporation from the canopy, E_c, (f) top layer soil moisture (0–0.1 m), $\Xi_{0-0.1m}$, (g) surface runoff, *R*, (h) potential groundwater recharge, *D*, and (i) total column soil moisture (0–3 m), Ξ_{0-3m}. Stippling shows where the changes are 95% significant, according to t-tests.

on average. Sylla et al. (2015) also predict a delay in the monsoon onset.

Values of $E_s + T$ (see Fig. 9d), mainly the result of decreased transpiration, is generally reduced in the future climate, except in the north in late spring and late summer, while changes in E_c (Fig. 9e) follow the changes in total rainfall as expected. *R* (Fig. 9g) is reduced in the south (4–9 N) from March to October but increased between 9 and 12 N in August and September. *D* (Fig. 9h) is reduced between 4 and 8 N from June to November but increased between 9 and 13 N from August to October. $\Xi_{0-0.1m}$ (Fig. 9f) is generally reduced throughout the year, while Ξ_{0-3m} (Fig. 9i) is generally greater, particularly between 9 and 13 N from October to June, but less in the south (4–7 N) from June to November.

4. Conclusions

Analysis of outputs from the global high-resolution climate model, UPSCALE, has shown significant changes for the future monsoon in the West Africa region, with higher temperatures over land, particularly in the Sahara, increased atmospheric humidity and increased cloud cover leading to greater net radiation. This results in an enhanced Saharan Heat Low in summer with greater south-north temperature and pressure gradients in West Africa and an altered large-scale circulation pattern. Greater overall rainfall is predicted within the region due to higher atmospheric humidity and stronger monsoon winds, with the summer wind direction coming more from the north over the western Sahel leading to reduced rainfall, but more from the south over the eastern Sahel leading to increased rainfall. The monsoon is predicted to move further to the north and both its onset and end will occur later in the summer for future climates. The higher air temperatures and increased humidity under future climatic conditions lead to more intense rain for large parts of West Africa, in particular the central and north-eastern parts.

JULES runs, driven with the UPSCALE atmospheric output, show that for the north-eastern parts of West Africa, increased future rainfall results in increased evapotranspiration, surface runoff, soil moisture content and potential recharge. However, with regards to the partitioning of the rainfall received, the fraction of total evapotranspiration *ET* (including interception evaporation *Ec*) is reduced as rainfall increases, partly due to the suppression of all evaporation and an increasing fraction going to throughfall. This results in greater fractions of the rainfall going to surface runoff and infiltrating into the soil layers resulting in increased potential recharge. Sensitivity experiments in which atmospheric CO_2 is kept at present levels, while the other atmospheric conditions are representative

of future climates, suggest that the primary driver of projected increased potential recharge is reduced transpiration, with the increase in rainfall a secondary factor. Changing vegetation type does appear to have a strong effect on potential recharge.

While the results appear robust, we acknowledge that differences in model structure and hydraulic parameter selection can affect water balance flux partitioning (see also Sorensen et al., 2014, and Weihermüller et al., 2021). However, we are currently conducting local-level runs with models such as the SWAP model (Van Dam et al., 2008) to study the water balance in this region in more detail, and our findings broadly confirm the results of this paper. Furthermore, the large-scale JULES setup assumes uniform, diffuse movement of water through the subsurface and does not allow the accumulation of water within topographic depressions, which facilitates focussed groundwater recharge. Focussed recharge is also likely to increase in line with predicted surface runoff, although predominantly due to increases in projected rainfall (Taylor et al., 2013; Cuthbert et al., 2019). Potential increases in groundwater recharge are important as the greater development of groundwater resources is considered as a key means for adaptation to climate change in West Africa.

CRediT authorship contribution statement

ECLB, AV, DMJM: Funding acquisition, Project administration, Conceptualization, Supervision, Methodology, Writing – review & editing. **PAC:** Data curation, Software, Visualization, Writing – original draft. **JPRS:** Writing – review & editing.

Declaration of Competing Interest

The authors declare that they have no known competing financial interests or personal relationships that could have appeared to influence the work reported in this paper.

Acknowledgements

This study is part of the project BRAVE (Building understanding of climate variability into planning of groundwater supplies from low storage aquifers in Africa), funded within the Unlocking the Potential of Groundwater for the Poor (UPGro) Programme by the UK Natural Environment Research Council, Economic and Social Research Council and the Foreign Commonwealth and Development Office (Grants NE/M008983/1 and NE/M008827/1). We thank Prof. Pier Luigi Vidale for supplying the UPSCALE data and his guidance with regards to the analysis of the data. David Macdonald and James Sorensen publish with the permission of the Executive Director, British Geological Survey and acknowledge support from the ODA National Capability Grant NE/R000069/1 (Geoscience for Sustainable Futures) for their contribution to the writing up of this work. Emily Black acknowledges the support of the National Centre for Atmospheric Science via the NERC/GCRF programme Atmospheric hazard in developing countries: risk assessment and early warning (ACREW). The sponsors of this work played no role in the study design; in the collection, analysis and interpretation of data; in the writing of the paper; and in the decision to submit the article for publication.

Declaration of Competing Interest

The authors declare that they do not have a conflict of interest.

Appendix A. Supporting information

Supplementary data associated with this article can be found in the online version at doi:10.1016/j.ejrh.2022.101076.

References

Adelana, M., MacDonald, A.M., 2008. Groundwater research issues in Africa. ⟨https://doi.org/10.1201/9780203889497.ch1⟩.

Allen, R.G., Pereira, L.S., Raes, D., Smith, M., 1998. Crop Evapotranspiration-Guidelines for Computing Crop Water Requirements. FAO Irrigation and Drainage, Paper 56, Food and Agriculture Organization of the United Nations (FAO), Rome.

Ascott, M.J., Macdonald, D.M.J., Black, E., Verhoef, A., Nakohoun, P., Tirogo, J., Sandwidi, W.J.P., Bliefernicht, J., Sorensen, J.P.R., Bossa, A.Y., 2020. In situ observations and lumped parameter model reconstructions reveal intra-annual to multidecadal variability in groundwater levels in sub-Saharan Africa. Water Resour. Res. 56 https://doi.org/10.1029/2020WR028056 (e2020WR028056).

Berthou, S., Rowell, D.P., Kendon, E.J., Roberts, M.J., Stratton, R.A., Crook, J.A., Wilcox, C., 2019. Improved climatological precipitation characteristics over West Africa at convection-permitting scales. Clim. Dyn. 53, 1991–2011. https://doi.org/10.1007/s00382-019-04759-4.

Best, M.J., Pryor, M., Clark, D.B., Rooney, G.G., Essery, R.L.H., Menard, C.B., Edwards, J.M., Hendry, M.A., Porson, A., Gedney, N., Mercado, L.M., Sitch, S., Blyth, E., Boucher, O., Cox, P.M., Grimmong, C.S.B., Harding, R.J., 2011. The joint UK land environment simulator (JULES), model description – Part 1: energy and water fluxes. Geosci. Model Dev. Discuss. 4, 677–699. https://doi.org/10.5194/gmdd-4-595-2011.

Bianchi, M., MacDonald, A.M., Macdonald, D.M.J., Asare, E.B., 2020. Investigating the productivity and sustainability of weathered basement aquifers in tropical Africa using numerical simulation and global sensitivity analysis. Water Resour. Res. 56 https://doi.org/10.1029/2020WR027746 (e2020WR027746).

Bichet, A., Diedhiou, A., 2018. West African Sahel has become wetter during the last 30 years, but dry spells are shorter and more frequent. Clim. Res. https://doi.org/10.3354/cr01515.

Black, E., Pinnington, E., Wainwright, C., Lahive, F., Quaife, T., Allan, R.P., Cook, P., Daymond, A., Hadley, P., McGuire, P.C., Verhoef, A., Vidale, P.L., 2021. Cocoa plant productivity in West Africa under climate change: a modelling and experimental study. Environ. Res. Lett. 16, 014009 https://doi.org/10.1088/1748-9326/abc3f3.

Brooks, R.H., Corey, A.T., 1964. Hydraulic Properties of Porous Media, Hydrol. Paper No. 3. Colorado State Univ., Fort Collins, CO.
Clark, D.B., Mercado, L.M., Sitch, S., Jones, C.D., Gedney, N., Best, M.J., Pryor, M., Rooney, G.G., Essery, R.L.H., Blyth, E., Boucher, O., Harding, R.J., Cox, P.M., 2011. The joint UK land environment simulator (JULES), model description – Part 2: carbon fluxes and vegetation dynamics. Geosci. Model Dev. Discuss. 4, 641–688. https://doi.org/10.5194/gmdd-4-641-2011.
Collatz, G.J., Ball, J.T., Grivet, C., Berry, J.A., 1991. Physiological and environmental regulation of stomatal conductance, photosynthesis, and transpiration: a model that includes a laminar boundary layer. Agric. For. Meteor. 54, 107–136. https://doi.org/10.1016/0168-1923(91)90002-8.
Cook, K.H., Vizy, E.K., 2015. Detection and analysis of an amplified warming of the Sahara Desert. J. Clim. 28, 6560–6580. https://doi.org/10.1175/JCLI-D-14-00230.1.
Cooper, P.J., Coe, R., 2011. Assessing and addressing climate-induced risk in sub-Saharan rainfed agriculture: foreword to a special issue of experimental agriculture. Exp. Agric. 47 (2), 179–184. https://doi.org/10.1017/S0014479711000019.
Coulibaly, N., Coulibaly, T.J.H., Mpakama, Z., Savane, I., 2018. The impact of climate change on water resource availability in a trans-boundary basin in West Africa: the case of Sassandra. Hydrology 5, 12. https://doi.org/10.3390/hydrology5010012.
Cuthbert, M.O., Taylor, R.G., Favreau, G., Todd, M.C., Shamsudduha, M., Villholth, K.G., MacDonald, A.M., Scanlon, B.R., Kotchoni, D.O.V., Vouillamoz, J.-M., Lawson, F.M.A., Adjomayi, P.A., Kashaigili, J., Seddon, D., Sorenson, J.P.R., et al., 2019. Observed controls on resilience of groundwater to climate variability in sub-Saharan Africa. Nature 572 (7768), 230–234. ISSN 0028-0836.
Dardel, C., Kergoat, L., Hiernaux, P., Mougin, E., Grippa, M., Tucker, C.J., 2014. Re-greening Sahel: 30 years of remote sensing data and field observations (Mali, Niger). Remote Sens. Environ. 140, 350–364. https://doi.org/10.1016/j.rse.2013.09.011.
Diallo, I., Giorgi, F., Deme, A., Tall, M., Mariotti, L., Gaye, A.T., 2016. Projected changes of summer monsoon extremes and hydroclimatic regimes over West Africa for the twenty-first century. Clim. Dyn. 47, 3931–3954. https://doi.org/10.1007/s00382-016-3052-4.
Dunning, C.M., Allan, R.P., Black, E., 2017. Identification of deficiencies in seasonal rainfall simulated by CMIP5 climate models. Environ. Res. Lett. 12, 114001 https://doi.org/10.1088/1748-9326/aa869e.
Favreau, G., Cappelaere, B., Massuel, S., Leblanc, M., Boucher, M., Boulain, N., Leduc, C., 2009. Land clearing, climate variability, and water resources increase in semiarid southwest Niger: A review. Water Resour. Res. 45 (7).
Fitzpatrick, R.G.J., Parker, D.J., Marsham, J.H., Rowell, D.P., Guichard, F.M., Taylor, C.M., Cook, K.H., Vizy, E.K., Jackson, L.S., Finney, D., Crook, J., Stratton, R., Tucker, S., 2020. What drives the intensification of mesoscale convective systems over the West African Sahel under climate change. J. Clim. 33, 3151–3172. https://doi.org/10.1175/JCLI-D-19-0380.1.
Gaetani, M., Janicot, S., Vrac, M., Famien, A.M., Sultan, B., 2020. Robust assessment of the time of emergence of precipitation change in West Africa. Nat. Sci. Rep. https://doi.org/10.1038/s41598-020-63782-2.
Ibrahim, B., Karambiri, H., Polcher, J., Yacouba, H., Ribstein, P., 2014. Changes in rainfall regime over Burkina Faso under the climate change conditions simulated by 5 regional climate models. Clim. Dyn. 42 (5–6), 1363–1381.
Jasechko, S., Taylor, R.G., 2015. Intensive rainfall recharges tropical groundwaters. Environ. Res. Lett. 10 (12), 124015 https://doi.org/10.1088/1748-9326/10/12/124015.
Jung, G., Kunstmann, H., 2007. High-resolution regional climate modeling for the Volta region of West Africa. J. Geophys. Res. 112, D23108 https://doi.org/10.1029/2006JD007951.
Kamga, A.F., Jenkins, G.S., Gaye, A.T., Garba, A., Sarr, A., Adedoyin, A., 2005. Evaluating the national center for atmospheric research climate system model over West Africa: present-day and the 21st century A1 scenario. J. Geophys. Res. 110, D03106 https://doi.org/10.1029/2004JD004689.
Kendon, E.J., Stratton, R.A., Tucker, S., Marsham, J.H., Berthou, S., Rowell, D.P., Senior, C.A., 2019. Enhanced future changes in wet and dry extremes over Africa at convection-permitting scale. Nat. Commun. 10, 1794 https://doi.org/10.1038/s41467-019-09776-9.
Kirschbaum, M.U.F., McMillan, A.M.S., 2018. Warming and elevated CO_2 have opposing influences on transpiration. Which is more important? Curr. For. Rep. 4 (2), 51–71. https://doi.org/10.1007/s40725-018-0073-8.
Krol, M.S., de Vries, M.J., van Oel, P.R., de Araújo, J.C., 2011. Sustainability of small reservoirs and large scale water availability under current conditions and climate change. Water Resour. Manag. 25 (12), 3017–3026. https://doi.org/10.1007/s11269-011-9787-0.
Marsham, J.H., Dixon, N.S., Garcia-Carreras, L., Lister, G.M.S., Parker, D.J., Knippertz, P., Birch, C.E., 2013. The role of moist convection in the West African monsoon system: Insights from continental-scale convection-permitting simulations. Geophys. Res. Lett. 40, 1843–1849. https://doi.org/10.1002/grl.50347.
Marthews, T., Quesada, C.A., Galbraith, D.R., Malhi, Y., Mullins, C.E., Hodnett, M.G., Dharssi, I., 2014. High-resolution hydraulic parameter maps for surface soils in tropical South America. NERC Environ. Inf. Data Cent. https://doi.org/10.5285/4078678b-768f-43ff-abba-b87712f648e9.
Maynard, K., Royer, J.F., Chauvin, F., 2002. Impact of greenhouse warming on the West African summer monsoon. Clim. Dyn. 19, 499–514. https://doi.org/10.1007/s00382-002-0242-z.
Mengis, N., Keller, D.P., Eby, M., Oschlies, A., 2015. Uncertainty in the response of transpiration to CO_2 and implications for climate change. Environ. Res. Lett. 10 (9) https://doi.org/10.1088/1748-9326/10/9/094001.
Meynadier, R., Bock, O., Guichard, F., Boone, A., Roucou, P., Redelsperger, J.L., 2010a. West African monsoon water cycle: 1. A hybrid water budget data set. J. Geophys. Res. 115, D19106 https://doi.org/10.1029/2010JD013917.
Meynadier, R., Bock, O., Gervois, S., Guichard, F., Redelsperger, J.L., Agusti-Panareda, A., Beljaars, A., 2010b. West African Monsoon water cycle: 2. Assessment of numerical weather prediction water budgets. J. Geophys. Res. 115, D19107 https://doi.org/10.1029/2010JD013919.
Mizielinski, M.S., Roberts, M.J., Vidale, P.L., Schiemann, R., Demory, M.-E., Strachan, J., Edwards, T., Stephens, A., Lawrence, B.N., Pritchard, M., Chiu, P., Iwi, A., Churchill, J., del Cano Novales, C., Kettleborough, J., Roseblade, W., Selwood, P., Foster, M., Glover, M., Malcolm, A., 2014. High-resolution global climate modelling: the UPSCALE project, a large-simulation campaign. Geosci. Model Dev. 7, 1629–1640. https://doi.org/10.5194/gmd-7-1629-2014.
Naabil, E., Lamptey, B.L., Arnault, J., Olufayo, A., Kunstmann, H., 2017. Water resources management using the WRF-Hydro modelling system: case-study of the Tono dam in West Africa. J. Hydrol.: Reg. Stud. 12, 196–209. https://doi.org/10.1016/j.ejrh.2017.05.010.
Odoulami, R.C., Akinsanola, A.A., 2018. Recent assessment of West African summer monsoon daily rainfall trends. Weather Mag. 73 (9), 283–287. https://doi.org/10.1002/wea.2965.
Panthou, G., Vischel, T., Lebel, T., 2014. Recent trends in the regime of extreme rainfall in the Central Sahel. Int. J. Climatol. 34, 3998–4006. https://doi.org/10.1002/joc.3984.
Panthou, G., Lebel, T., Vischel, T., Quantin, G., Sane, Y., Ba, A., Ndiaye, O., Diongue-Niang, A., Diopkane, M., 2018. Rainfall intensification in tropical semi-arid regions: the Sahelian case. Environ. Res. Lett. 13, 064013 https://doi.org/10.1088/1748-9326/aac334.
Roehrig, R., Bouniol, D., Guichard, F., Hourdin, F., Redelsperger, J.L., 2013. The present and future of the West African monsoon: a process-oriented assessment of CMIP5 simulations along the AMMA transect. J. Clim. 26, 6471–6505. https://doi.org/10.1175/JCLI-D-12-00505.1.
Sacre Regis, D.M., Mouhamed, L., Kouakou, K., Adeline, B., Arona, D., Houebagnon Saint, C.J., Koffi Claude, K.A., Talnan Jean, C.H., Salomon, O., Issiaka, S., 2020. Using the CHIRPS dataset to investigate historical changes in precipitation extremes in West Africa. Climate 2020 (8), 84. https://doi.org/10.3390/cli8070084.
Sorensen, J.P.R., Finch, J.W., Ireson, A.M., Jackson, C.R., 2014. Comparison of varied complexity models simulating recharge at the field scale. Hydrol. Process. 28 (4), 2091–2102. https://doi.org/10.1002/hyp.9752.
Sultan, B., Gaetani, M., 2016. Agriculture in West Africa in the twenty-first century: climate change and impacts scenarios, and potential for adaptation. Front. Plant Sci. 7 (1262) https://doi.org/10.3389/fpls.2016.01262.
Sylla, M.B., Giorgi, F., Pal, J.S., Gibba, P., Kebe, I., Nikiema, M., 2015. Projected changes in the annual cycle of high-intensity precipitation events over West Africa for the late twenty-first century. J. Clim. 28, 6475–6488. https://doi.org/10.1175/JCLI-D-14-00854.1.
Sylla, M.B., Pal, J.S., Faye, A., Dimobe, K., Kunstmann, H., 2018. Climate change to severely impact West African basin scale irrigation in 2 °C and 1.5 °C global warming scenarios. Nat. Sci. Rep. https://doi.org/10.1038/s41598-018-32736-0.
Taylor, C.M., Belusic, D., Guichard, F., Parker, D.J., Vischel, T., Bock, O., Harris, P.P., Janicot, S., Klein, C., Panthou, G., 2017. Frequency of extreme Sahelian storms tripled since 1982 in satellite observations. Nature 544, 475–478. https://doi.org/10.1038/nature22069.

Taylor, R., Todd, M., Kongola, L., et al., 2013. Evidence of the dependence of groundwater resources on extreme rainfall in East Africa. Nat. Clim. Change 3, 374–378. https://doi.org/10.1038/nclimate1731.
Todzo, S., Bichet, A., Diedhiou, A., 2019. Intensification of the hydrological cycle expected in West Africa over the 21st century. Earth Syst. Dyn. https://doi.org/10.5194/esd-2019-38.
UNECA, 2015. Report on Sustainable Development Goals for the West Africa Subregion. United Nations Economic Commission for Africa, Addis Ababa, Ethiopia.
Van Dam, J.C., Groenendijk, P., Hendriks, R.F.A., Kroes, J.G., 2008. Advances of modeling water flow in variably saturated soils with SWAP. Vadose Zone J. 7, 640–653.
Van Genuchten, M.Th., 1980. A closed form equation for predicting the hydraulic conductivity of unsaturated soils. Soil Sci. Soc. Am. J. 44, 892–898.
Vellinga, M., Roberts, M., Vidale, P.L., Mizielinski, M.S., Demory, M.E., Schiemann, R., Strachan, J., Bain, C., 2016. Sahel decadal rainfall variability and the role of model horizontal resolution. Geophys. Res. Lett. https://doi.org/10.1002/2015GL066690.
Walters, D.N., et al., 2011. The Met Office unified model global atmosphere 3.0/3.1 and JULES global land 3.0/3.1 configurations. Geosci. Model Dev. 4, 919–941. https://doi.org/10.5194/gmd-4-919-2011.
Weihermüller, L., Lehmann, P., Herbst, M., Rahmati, M., Verhoef, A., Or, D., Jaques, D., Vereecken, H., 2021. Choice of pedotransfer functions matters when simulating soil water balance fluxes. J. Adv. Model. Earth Syst. 13 (3) https://doi.org/10.1029/2020MS002404 (ISSN: 1942-2466).
Xu, Z., Jiang, Y., Jia, B., Zhou, G., 2016. Elevated-CO_2 response of stomata and its dependence on environmental factors. Front. Plant Sci. https://doi.org/10.3389/fpls.2016.00657.

Further reading

Alamirew, N.K., Todd, M.C., Ryder, C.L., Marsham, J.M., Wang, Y., 2017. The summertime Saharan heat low: sensitivity of the radiation budget and atmospheric heating to water vapor and dust aerosol. Atmos. Chem. Phys. Discuss. https://doi.org/10.5194/acp-2017-397.
Anayah, F., Kaluarachchi, J.J., 2009. Groundwater Resources of Northern Ghana: Initial Assessment of Data Availability. College of Engineering, Utah State University.
Birch, C.E., Parker, D.J., Marsham, J.H., Copsey, D., Garcia-Carreras, L., 2014. A seamless assessment of the role of convection in the water cycle of the West African Monsoon. J. Geophys. Res. Atmos. 119, 2890–2912. https://doi.org/10.1002/2013JD020887.
Boone, A., de Rosnay, P., Balsamo, G., Beljaars, A., Chopin, F., Decharme, B., Delire, C., Ducharne, A., Gascoin, S., Grippa, M., Guichard, F., Gusev, Y., Harris, P., Jarlan, L., Kergoat, L., Mougin, E., Nasonova, O., Norgaard, A., Orgeval, T., Ottle, C., Poccard-Leclercq, I., Polcher, J., Sandholt, I., Saux-Picart, S., Taylor, C., Xue, Y., 2009. The AMMA land surface model intercomparison project (ALMIP). BAMS. https://doi.org/10.1175/2009BAMS2786.1.
Ewusi, A., Kuma, J.S.Y., 2014. Groundwater assessment for current and future water demand in the Daka catchment, Northern Region, Ghana. Nat. Resour. Res. 23, 4. https://doi.org/10.1007/s11053-014-9227-y.
Martin, N., van de Giesen, N., 2005. Spatial distribution of groundwater production and development potential in the Volta river basin of Ghana and Burkina Faso. Water Int. 30 (2), 239–249. https://doi.org/10.1080/02508060508691852.
Ndehedehe, C.E., Awange, J.L., Kuhn, M., Agutu, N.O., Fukuda, Y., 2017. Climate teleconnections influence on West Africa's terrestrial water storage. Hydrol. Process. 31, 3206–3224. https://doi.org/10.1002/hyp.11237.
Nicholson, S.E., 2013. The West African Sahel: a review of recent studies on the rainfall regime and its interannual variability. ISRN Meteorol. 1–32. https://doi.org/10.1155/2013/453521.